INSTITUTE
FOR
AEROSPACE STUDIES

UNIVERSITY OF TORONTO

THE EFFECT OF INCLINATION ON THE STROUHAL NUMBER AND OTHER WAKE PROPERTIES OF CIRCULAR CYLINDERS AT SUBCRITICAL REYNOLDS NUMBERS

by

J. Surry and D. Surry

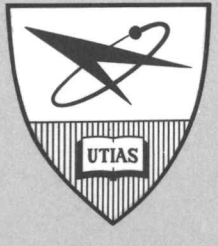

AUGUST 1967

UTIAS TECHNICAL NOTE No. 116

THE EFFECT OF INCLINATION ON THE STROUHAL NUMBER AND OTHER WAKE PROPERTIES OF CIRCULAR CYLINDERS AT SUBCRITICAL REYNOLDS NUMBERS

by

J. Surry and D. Surry

Manuscript received January 1967

AUGUST 1967

UTIAS TECHNICAL NOTE NO. 116

ACKNOWLEDGEMENTS

The authors would like to acknowledge Professor B. Etkin's initial suggestion for this investigation and his continued interest and encouragement.

Much credit is due to Mr. Hans Teunissen and Mr. Murray McLeod for their assistance in the reduction of data.

Financial support for this research was received from the National Research Council of Canada and from the U. S. A. F., R. T. D., under contract AF(33) 615-2305.

SUMMARY

A brief experimental investigation was made to determine the effect of inclination on the Strouhal Number of circular cylinders at Reynold's numbers from 4,000 to 65,000. It was found that the Strouhal Number based on the normal velocity component remained constant to a good approximation. Spectral techniques showed that the energy of the shed vortices dispersed in frequency and decreased in significance with increasing inclination, such that for angles less than 40^{o} the shedding energy was negligible compared to the general wake turbulence energy, at 7.5 diameters downstream from the cylinder.

Other wake properties were briefly investigated. These included the decay of the u-component of turbulence downstream and the behaviour of the wake spectra with inclination, speed and wake location.

TABLE OF CONTENTS

LIST OF SYMBOLS

B, V_o	calibration constants of Disa hot wire anemometer arising from King's Law, $V^2 = V_o^2 + B\sqrt{U}$
C_p	pressure coefficient, $C_p = \frac{P-P_o}{1/2 \rho U_o^2}$
C_Z	Z - force coefficient, $C_Z = \frac{Z}{1/2 \rho U_o^2 d}$
d	cylinder diameter
D	drag force/unit length of the cylinder
$e_G(f_c)$	r.m.s. output voltage from a filter with bandwidth G centered at f_c
f	frequency, cps.
f_c	centre frequency of filter
f_p	frequency at the peak of $\overline{\phi}$, i.e. the Strouhal shedding frequency
$g(f/f_c)$	normalized ($g(1) = 1$) mean square attenuation of a sine wave of frequency f passing through a filter of centre frequency f_c.
G	bandwidth of filter, $G = \int_o^\infty g\,d(f/f_c)$
K, K'	calibration factors - see section 2.3
L	lift force/unit length of the cylinder
N	force/unit length normal to the body axis
$P-P_o$	static pressure difference from free stream
q	dynamic pressure of free stream, $q = 1/2 \rho U_o^2$
R	peakiness factor - see section 2.3
Re	Reynold's Number, $R_e = \frac{Uod}{\nu}$
Re_S	Reynold's Number based on streamwise chord, $Re_S = \frac{U_o(d/\sin\phi)}{\nu}$
S	Strouhal Number, $S = \frac{f_p d}{U_o}$
t	force/unit length tangential to the body axis; time

U	total longitudinal velocity, $U = \bar{U} + u(t)$
$\bar{U}$	mean longitudinal velocity, $\bar{U} = \lim_{T\to\infty} \frac{1}{T} \int_0^T U \, dt$
u	fluctuating component of longitudinal velocity, $\bar{u} = 0$
$\sqrt{\bar{u}^2}$	r. m. s. value of u, $\sqrt{\bar{u}^2} = \left[\lim_{T\to\infty} \int_0^T u^2 \, dt\right]^{1/2}$
V	total voltage from Disa anemometer, $V = \bar{V} + v$ (t)
$\bar{V}$	mean value of V
v	fluctuating component of V
V_{rms}	r. m. s. value of v
x	distance downstream from the centre-line of the cylinder
y	lateral distance measured perpendicularly from the plane containing the cylinder axis and the mean velocity vector
$\frac{\Delta z}{z}$	fractional error in a quantity z
ϵ	ratio of experimentally determined spectral peak (using the narrow filter) to the local "base" spectrum level - see Appendix
η	amplitude gain of wave analyser and tape recorder system, $\eta = (\frac{e_\infty}{V_{rms}})$
ν	kinematic viscosity
ρ	air density
ϕ	angle of inclination with respect to the streamwise direction
$\underline{\phi}$	spectral density function, $\overline{u_w^2} = \int_0^\infty \underline{\phi} \, df$
$(\,)_n$	denotes a quantity based on the normal velocity component
$(\,)_o$	denotes a free stream value
$(\,)_w$	denotes a wake property
a, b, Δ, α	constants

I. INTRODUCTION AND REVIEW

Since vortex shedding from cylinders has important implications both fundamentally and in the design of structures a simple experiment was initiated in the summer of 1965 in order to examine the behaviour of the Strouhal number with inclination of the cylinder. After the experiments were completed the only other relevant material became available (Ref. 1). The latter, however, concerns a lower Reynolds number range than that examined here.

Understanding of the mechanism of vortex shedding has progressed little from Roshko's experimental work in 1954 (Ref. 2); hence prediction of the shedding frequency from other known properties of the flow about an arbitrary body cannot confidently be made. Roshko however did derive a semi-empirical relation which describes well the shedding from right cylinders with a variety of cross-sections.

The following sections discuss the known variations of wake properties with inclination angle. Then a discussion of vortex shedding from right cylinders leads into postulation of the form of the variation with inclination. The remaining work describes the experiment to test this hypothesis, and the results obtained. The results also yielded some insight into the effect of inclination on the mean wake velocity, on the wake turbulence energy, and the wake energy spectrum. Since the right cylinder was included in the angles tested, these results also contribute to the sparse knowledge about the wake immediately behind the 90^{o} cylinder.

1.1 The Effect of Inclination Angle on Wake Properties for Re from 10^4 to 10^5:

An earlier report (Ref. 3) presented the current knowledge of the properties of the airflow around a circular cylinder inclined to the wind at Re Numbers from 10^4 to 10^5. A summary of the relevant features follows.

In 1917, Relf and Powell (Ref. 4) measured the lift and drag on such cylinders. Their results showed that for subcritical flows to a good approximation, the forces are, respectively

$$L \propto \sin^2\phi \cos\phi$$

and

$$D \propto \sin^3\phi$$

or, in terms of the force normal to the cylinder axis,

$$N \propto \sin^2\phi \qquad \text{(Fig. 1.1)}$$

Since the normal velocity component

$$U_n = U_o \sin\phi$$

and, also $$N \propto U_o^2$$

Thus $$N \propto U_n^2$$

This suggests that the flow about the cylinder in planes normal to the axis is simply a function of the local normal velocity. The tangential force, t, was found negligibly small. The tangential velocity component simply results in a friction force. These results can be explained in terms of the laminar flow before separation being predictably only a function of U_n (Ref. 5).

However, two points arose in Ref. 3, indicating that although the "macro-properties" are functions of the normal velocity component only, the "micro-properties" of the wake are not as readily explained. First, Bursnall and Loftin (Ref. 6) made a pressure survey on cylinders inclined to the wind at both super- and sub- critical Reynolds numbers. For the latter conditions their results were similar to those of Relf and Powell, but they observed that the pressure in the wake, to a small extent, was not simply a function of the normal velocity, but rather

$$C_{p_w}(\phi) = C_{p_w}(90^o) \sin^2\phi + \triangle$$

where $\triangle$ is a constant.

The second point was that flow visualisation studies presented in Ref. 3 indicate a flow tangential to the cylinder in the wake just behind the separation line. It was postulated that these effects are due to the streamwise shearing action of the laminar flow external to the wake.

Hence the simple postulate of normal flow does not fully explain the flow properties around an inclined cylinder in this Reynolds number range. This is also evident in the following section.

1.2 The Effect of Inclination Angle on Wake Properties for Other Reynolds Number Ranges:

Two studies of different flow regimes have identified the Reynolds numbers at which transition between various regimes occurs as functions of the inclination angle. Hanson (Ref. 1) found that the critical Reynolds number at which stable shedding first occurred was approximately constant (40-50) with changing inclination, if based on the normal velocity component; i.e. at the transition point

$$Re_n = \frac{d(U_o \sin\phi)}{\nu} = \text{constant} \quad 90^o \geqslant \phi \geqslant 30^o$$

However Bursnall and Loftin found that the transition from laminar to turbulent boundary layers ahead of the wake, apparently occurred at a constant Reynolds number based on the streamwise chord: for $90^o \geqslant \phi \geqslant 30^o$

$$Re_S = \frac{U_o\, d/\sin\phi}{\nu} = \text{constant} \quad (3.8 \times 10^5)$$

This latter result may be due to the dependence of this flow transition on the length of the particle path which is roughly proportional to $(d/\sin\phi)$ for the inclined cylinder.

Hanson also measured the vortex shedding frequencies in the lower Reynolds number range for the inclined cylinders. He found that for any speed

$$f_p \propto \sin \phi$$

Thus if both the Strouhal and the Reynolds numbers were defined based on the normal velocity component, i. e.

$$S_n = \frac{f_p\, d}{U_o \sin \phi}$$

$$Re_n = \frac{(U_o \sin \phi)\, d}{\nu}$$

his results collapsed to the common curve:

$$S_n = 0.212 - 4.5/Re_n$$

For $\phi = 90^o$, $S_n = S$ and $Re_n = Re$ and the relation becomes:

$$S = 0.212 - 4.5/Re$$

as Roshko found in Reference 2 for Reynolds numbers between 50 and 150.

Thus, it appears that the relevant Reynolds number may depend on the particular flow property of interest for an inclined cylinder. In the following, the free stream Reynolds number ($\frac{U_\infty d}{\nu}$ is generally used, unless otherwise noted.

1. 3 Strouhal Shedding for Right Cylinders:

The Strouhal number has been measured throughout the range of Reynolds numbers from 50 to 10^7 for circular cylinders normal to the stream. A typical ensemble of results is shown in Figure 1. 2 taken from Reference 7. The variations of the Strouhal number across different Reynolds number regimes reflects other experimentally observed changes in the wake. Hanson's work described in section 1. 2 was in the region of stable regular vortex shedding. The following work lies in the region where the wake flow is quite irregular but where there is a dominant single frequency which is designated as the Strouhal frequency.

In terms of a wake energy spectrum; this Strouhal frequency is a discrete peak superimposed on a continuous spectrum across higher and lower frequencies. Taken from Reference 2 is a typical spectrum shown in Figure 1. 3. Such data also show that the energy at the shedding frequency relative to the total wake energy (the integral under the spectrum) decreases

rapidly downstream until at 48 diameters no discrete energy can be detected at the shedding frequency. Unlike at lower Reynolds numbers, the discrete energy has dissipated or transferred to other frequencies, and the remaining energy spectrum has a relatively smooth energy distribution. This continuous energy spectrum Roshko showed to be well fitted by the expression

$$a / (1+b^2 f^2)$$

In Ref. 8 Roshko developed a semiempirical relationship between the Strouhal number, the drag, and the wake pressure on a bluff cylinder. With any one of these parameters known the other two can be calculated. Consider the inclined cylinder in a flow of speed U_o: it has been shown that the pressures and forces on the body are approximately the same as those on a right cylinder in a flow of speed $U_o \sin(\phi)$. That is, if the coefficients are defined in terms of the geometry of such a right cylinder system they are constant independent of the original inclination. In the inclined system

$$C_{p_w}(\phi) \triangleq \frac{P - P_o}{1/2\, \rho\, U_o^2} = C_{p_w}(90) \sin^2 \phi$$

$$C_N(\phi) \triangleq \frac{N}{1/2\, \rho\, U_o^2\, d} = C_N(90) \sin^2 \phi$$

while in the right cylinder system (primed) with $U' = U_o \sin \phi$

$$C'_{p_w}(\phi) \triangleq \frac{P - P_o}{1/2\, \rho\, U'^2} = \frac{P - P_o}{1/2\, \rho\, U_o^2 \sin^2 \phi} = \frac{C_{pw}(\phi)}{\sin^2 \phi} = C_p(90^o)$$

$$C'_d(\phi) \triangleq \frac{D'}{1/2\, \rho\, U'^2} = \frac{N}{1/2\, \rho\, U_o^2 \sin^2 \phi} = \frac{C_N(\phi)}{\sin^2 \phi} = C_N(90^o)$$

Note that in the primed system the drag on the cylinder is the normal force component, N. Thus if the drag and pressure coefficients (which are both constant) fully define the Strouhal number,

$$\text{approx.} \quad S' \triangleq \frac{f_p\, d}{U'} = \frac{f_p\, d}{U_o \sin \phi} \doteq 0.2 \quad \text{(for right cylinders)}$$

Then in the inclined system

$$S \triangleq \frac{f_p\, d}{U_o} = S' \sin \phi \doteq 0.2 \sin \phi$$

Thus we might anticipate that the Strouhal number will decrease as the sine of the inclination angle, as Hanson did in fact find at low Reynolds numbers.

II. EXPERIMENTAL TECHNIQUES

The experiments were performed in the UTIAS Subsonic wind tunnel which is a closed circuit tunnel providing test speeds up to 200 fps with a turbulence level of 0.3%. The free stream dynamic pressure was

measured with a Betz water manometer. Five speeds were used for each angle of the cylinder, covering the Reynolds number range of 4,500 to 63,000.

2.1 Inclined Cylinders:

The cylinders, of fixed diameter (0.91"), were cut to length to meet the top and the bottom of the wind tunnel test section, while presenting a range of fixed inclination angles to the wind, Figure 2.1a. The ends were sealed flush with the tunnel surfaces and aligned on the test section centre lines. The angles used were 90^{o}, 75^{o}, 64^{o}, 52^{o}, 42^{o}, 35^{o}.

Another arrangement was made for the very shallow angles. As in the sketch of Figure 2.1b, a single cylinder of the same diameter as those in the previous tests, was pivoted at each end at its juncture with two false walls. The cylinder and the false walls were aligned with the stream such that the horizontal cylinder formed the required angle and the walls were parallel to the stream. The junctions between the cylinder and the walls were filled to simulate the flush joint as used in the first part of the test. The angles used were 42^{o}, 35^{o} (to overlap the first tests), 25^{o}, 15^{o} and 10^{o}.

2.2 Instrumentation:

2.2.1 Location of the Hot Wire Probe:

The principal location of the hot wire used to investigate the wake was at a fixed downstream, off centre-line position, as shown in Figure 2.2. The downstream location was chosen to accommodate very shallow angles of the cylinder, while still remaining in a region of measurable turbulence amplitude. The off-centre location was chosen to place the probe directly in the vortex path, originating from one side of the cylinder. The effect of varying this wake location was measured in a series of tests for one cylinder angle. The results are presented, where pertinent, in Section 3.

Preliminary tests examined the feasibility of measuring the vortex shedding frequency using a hot wire placed in the fluctuating potential flow upstream of the separation point near the surface of the cylinder. This technique had been used successfully in previous tests. However, the inclination introduced geometrical difficulties and a rapidly decreasing signal with decreasing angle. Thus the wake location was adopted which overcame the physical mounting problems and allowed a comparison between the intensities of the vortex shedding and the general wake turbulence.

The wire was always mounted perpendicular to the free stream velocity, and parallel to the plane defined by the cylinder axis and the streamwise direction. The wire thus measures only the streamwise velocity component.

2.2.2 Measuring Technique:

Figure 2.3 schematically indicates the electronic layout. The DISA Constant Temperature Anemometer used was 'unlinearised' and yielded directly the d.c. and r.m.s. voltages of the bridge output. The probes were calibrated by comparing known wind speeds measured by a standard water pressure manometer, with the d.c. voltage output. All the probes obeyed King's Law over the experimental range and thus the local linearisation approximation was used to find the mean square turbulent velocity from the r.m.s. voltage. The air temperature was recorded and at most varied $10^{o}F$, generally less than $5^{o}F$, thus temperature corrections for the probes were ignored.

The high-pass filter shown had a cut-off at 1 cps, in order to block a spurious d.c. voltage from the DISA. The fluctuating signal was amplified with a low noise 'd.c. - 10kc' amplifier. The resulting signal was observed on an oscilloscope, taped when records were desired, and read on an rms meter. The FM tape recorder had a flat response up to 1250 cps.

2.3 Data Reduction:

The free stream velocity was found from the dynamic pressure:

$$U_o = \sqrt{\frac{2q}{\rho}}$$

The mean wake velocity was found from the probe signal d.c. level $\overline{V}$, by King's Law:

$$\overline{U}_w = \left(\frac{\overline{V}^2 - V_o^2}{B}\right)^2$$

where V_o and B are constants of the probe at given operating conditions. The percent turbulence was calculated from a manipulation of King's Law:

$$\% \text{ Turbulence} \triangleq \frac{100\sqrt{\overline{u_w^2}}}{\overline{U}_w} = 100\, V_{rms}\left(\frac{4\overline{V}}{\overline{V}^2 - V_o^2}\right)$$

where V_{rms} is the rms value of the probe signal.

To obtain wake spectra the taped signals were analysed with a wave analyser. Two filter widths were used, which were Broad (about 29%) and Narrow (about 10%), where the width

$$G \triangleq \int_0^\infty e_o^2/e_i^2 \; d(f/f_c)$$

and e_o/e_i is the normalised attenuation at any frequency when the filter is centred at f_c. The wider filter was used for a coarse spectral analysis and the narrow filter was used to study areas of the spectrum which were apparently rapidly changing. The spectral density function is given by:

$$\overline{\phi} = \frac{K'}{G\eta^2} \frac{e_G^2(f_c)}{f_c}$$

where $e_G(f_c)$ is the r. m. s. output voltage of the filter (width G) centered at the frequency f_c (in the following the subscript 'c' is dropped). η is the system (tape recorder and wave analyser) gain, calculated from a 60 cps calibration signal. K' is a function of the wind speed and the hot wire calibration. Anticipating a function of the dynamic pressure, division is made by $\overline{U_w}^2$

$$\overline{\phi} \Big/ \overline{U_w}^2 = (K/G\eta^2) \frac{e_G^2(f)}{f}$$

where

$$K = \frac{K'}{\overline{U_w}^2} = \left(\frac{4\overline{V}}{\overline{V^2} - V_o^2} \right)^2$$

The peak value of $\overline{\phi}(f)/\overline{U_w}^2$ was used to define the Strouhal frequency f_p. The Strouhal number is defined as $S \triangleq \frac{f_p d}{U_o}$. A 'peakiness' factor was defined to indicate the sharpness of this peak:

$$R \triangleq \frac{e_N^2(f_p)}{e_B^2(f_p)}$$

This is effectively the ratio of the energy passing through the Narrow filter to that passing through the Broad filter. Note that if the spectrum had a single discrete peak at f_p $R_{peak} = 1.0$; if the spectrum were flat

$$R_{flat} = \frac{G_N}{G_B} = 0.363 \quad \text{(in this experiment)}$$

and if the spectrum had a single discrete peak superimposed on a flat 'base' spectrum,

$$R_{comb.} = \frac{(G_N/G_B)\epsilon}{1+(G_N/G_B)(\epsilon - 1)}$$

where ϵ is the measured ratio of the peak to base heights of the 'combined' flat and peaked spectrum (see Appendix).

III. ANALYSIS OF THE RESULTS

The hot wire signal was monitored during the experiment on an oscilloscope both in its 'pure' state and after it had been passed through a wave analyser set at the dominant signal frequency. A typical example is shown in Figure 3.1 for a 90° cylinder, where the upper trace of each pair represents the instantaneous filtered value of the lower complete signal. (Note the gains on the two channels are not the same). The three pairs represent three increasing speeds from top to bottom. The increase of the predominant Strouhal frequency with speed is immediately apparent, and is

associated with a shift in the entire spectrum of the signal to higher frequencies. The characteristic modulation of the Strouhal frequency is evident, especially at the highest speed, and was observed for all angles of inclination where a Strouhal frequency could be identified. As may be observed in the photograph, the intermediate speed seemed to yield the most readily identifiable Strouhal frequency in the unfiltered signal; however, as inclination was increased the Strouhal frequency soon visually disappeared into the accompanying random turbulence - even at angles of 60°.

3.1 Gross Wake Features:

3.1.1 Mean Wake Velocities:

Figure 3.2 shows the variation of the ratio of wake velocity to free stream with the free stream velocity, for each angle tested by the tunnel-spanning cylinders.

Before discussing the significance of the results, the errors in the measurements should be estimated. From King's Law

$$\bar{U} \propto (\bar{V}^2 - V_o^2)^2$$

this relation will generate large errors in mean velocities despite care taken in measurement of the probe voltage, V. In this case

$$\frac{\Delta \bar{U}}{\bar{U}} = 2\left[\frac{\Delta (\bar{V}^2 - V_o^2)}{\bar{V}^2 - V_o^2} + \frac{\Delta B}{B}\right]$$

where $\Delta B/B$ is the error in the calibrated slope B (1%). The maximum error in $(\bar{V}^2 - V_o^2)$ varied from 5.5 to 3.0% as the speed increased thus the error in the mean velocity is 13 to 8%. The error in the free stream velocity measurement is about 1%, thus the total maximum error in $\bar{U}_w/U_o$ is 14 to 9%. The probable error will be much less than these values.

Comparison of the results cannot be made with those of other workers since the point of measurement was 7.4 ($\pm$1%) diameters downstream from the cylinder axis, while other data is only available for greater than 80 diameters downstream.

The curves indicate a strong Reynolds number dependence, especially between Re = 4500 and 25000. This might be anticipated from the well documented variation of the wake pressure and drag coefficients across this Reynolds number range. Other variations apparent in the figure are not significantly greater than the error of measurement of $\bar{U}_w/U_o$, as discussed above. However $\bar{U}_w/U_o$ does tend to decrease as the Reynolds number increases further.

The variation with ϕ is not clearly defined but for the smaller

angles $\overline{U}_w / U_o$ tends toward unity as might be expected, due to the known decrease in the drag coefficient with inclination.

Thus, in summary, the mean wake velocity at this wake position is between 70 and 90% of the free stream velocity, and is dependent on the free stream Reynolds number and the inclination of the cylinder.

3.1.2 Wake Turbulence:

Figure 3.3 presents the percent turbulence measured as a function of the cylinder inclination angle for two free stream speeds. As before the error of measurement should be presented before discussing these results. From the functions in Section 2, the error in '% Turbulence' is

$$\frac{\Delta V_{rms}}{V_{rms}} + \frac{\Delta \overline{V}}{\overline{V}} + \frac{\Delta (V^2 - V_o^2)}{V^2 - V_o^2}$$

neglecting the effect of the local linearisation. The errors in the probe voltages $\Delta V_{rms}/V_{rms}$ and $\Delta \overline{V}/\overline{V}$ were about 1.5 and 2.5%, respectively. Thus the estimated maximum error in '% Turbulence' is 7.0% for the cases shown. Since for the highest angles the turbulence level is quite high at about 20%, consideration of the error due to the linearisation assumption should also be made. Hinze (Ref. 9) indicates that for the Constant Temperature system the experimental value is about 3% too high when the turbulence level is 20%. This latter error is systematic and thus does not contribute to the scatter of the data - only the shape of the mean curve as the turbulence decreases.

The results tend to indicate a small dependence on speed, but the difference falls within the estimated maximum 14.0 % of each other for any one angle. There is a significant decrease in the turbulence level with decreasing angle. Also plotted are the curves A sin ϕ and B sin $^{3/2}\phi$, where A and B have been chosen for best fit. The data are within experimental error of either curve although the inflection in the experimental data suggests the second curve to be more suitable. The following is the reason for anticipating the sin $^{3/2}\phi$ relationship.

The turbulence energy at any point downstream of a bluff body would be expected to depend on the energy input per unit volume at the body, which is proportional to $C_D U_o^2$. Hence, considering the portion of the turbulent energy represented by the u-component, a relationship of the form

$$\overline{u_w^2} = U_o^2 \; C_D \, f(x/d)$$

might be expected, where f is some unknown function of the geometrical parameter x/d. Thus in the case of the inclined cylinder,

$$\frac{\overline{u_w^2}}{U_o^2} \propto C_D(\phi) = C_D(90^o) \sin^3 \phi \quad \text{(from Sec. 1.2)}$$

Thus the '% Turbulence'

$$\frac{\sqrt{\overline{u_w^2}}}{U_w} \propto \sin^{3/2} \phi$$

assuming U_w/U_o is unaffected by the inclination, which, as seen in Section 3.1.1, is a fair approximation for first order estimates.

Note that the agreement between the data and the $\sin^{3/2} \phi$ law depends on the validity of

$$C_D(\phi) = C_D(90^o) \sin^3 \phi$$

for small ϕ, where it is in most doubt. For instance the experimental variation in C_{p_w} noted previously (Section 1.1) implies a more complex form for the drag coefficient, which increases in significance at small ϕ.

3.1.3 The Effect of Position in The Wake Behind a Right Cylinder:

To investigate the effect of probe location the mean wake velocities and '% Turbulence' were found at varying positions with a right cylinder. Figure 3.4 indicates the variation in these parameters for two different free stream speeds.

The mean wake velocity does not alter significantly over eleven diameters downstream, though a decrease is indicated immediately behind the cylinder. Since at the cylinder rear surface the mean velocity must be zero this decrease is to be expected. Also as anticipated this velocity ratio apparently increases as the probe moves out toward the edge of the wake. The ratio shows a slight Reynolds number effect as in Section 3.1.1.

The '% Turbulence' decreases with increasing distance from the cylinder and from the centre line. This agrees with previous results investigating the decay of turbulence behind a bluff cylinder. The interesting fact is that the majority of the other spectral studies have been restricted to the region of turbulence which is more than 80 diameters downstream, where the flow is approaching 'self-preservation' and similarity considerations can be applied (Ref. 10). However in the region investigated here the turbulence already appears to follow the decay law:

$$\frac{\overline{U}_w^2}{u_w^2} \propto (x - x_o)$$

as shown in Figure 3.5.

3.2 Predominant Features of the Wake Spectra:

3.2.1 Variation of the Wake Spectra with Angle:

When the spectral density function is plotted against the frequency for different values of ϕ at one speed, the curves have similarities, but reveal a monotonic change with ϕ (Figure 3,6). All the curves have a peak energy, but the corresponding frequency and height decrease while the width increases with inclination. No second harmonic of the Strouhal shedding frequency was observed, in agreement with Roshko's results at this Reynolds number. It is possible, however, that the second harmonic was too weak to show any peculiarity in the spectrum with the Broad filter, and this frequency region was not studied in detail with the Narrow filter; on further inspection the spectra do suggest a slight 'hump' at the frequency twice that of the peak.

At low frequencies the spectra level out, but at decreasing levels with angle. At high frequencies the energy curves have a common slope ($\pm$ 5%) on the logarithmic plot, i.e.

$$\overline{\phi} / U_w^2 \propto f^{-2.0} \qquad \text{for } f \geq 4f_p$$

This is the same as the relation Roshko fitted to his data

$$\overline{\phi} = \frac{a}{1 + b^2 f^2}$$

wherein, when f gets large

$$\overline{\phi} = a/b^2 f^2$$

Though not illustrated the spectra show a strong speed dependence as would be expected.

3.2.2 Strouhal Numbers:

From spectra as in Figure 3.6, the peak frequency was identified for all speeds and angles tested. For cases of small inclination, the peak frequencies were easily found; however, for larger inclinations the peaks were 'smudged' across the 'base' spectrum - which was falling rapidly. In these cases, the spectrum was considered to be a superposition of a 'base' spectrum and an addition 'hump' due to the dispersed Strouhal shedding. To obtain the true peak of this hump, the difference was taken between the measured spectrum and an estimate for the base spectrum. This resulted in a shedding frequency that was slightly higher than that apparent from the composite spectrum.

Figure 3.7a indicates the variation of the Strouhal number

$S = f_p d/U_o$ with the angle of inclination of the cylinder for all speeds. The shedding frequency, f_p, and hence the Strouhal number decreases as the angle of inclination becomes shallower. The scatter in the data at low angles is due primarily to the uncertainty in f_p caused by the flattening of the spectral peaks with inclination shown previously. This effect is elaborated in Section 3.2.3 and appropriate error bars appear in Figure 3.7c.

If the Strouhal number is redefined using the normal velocity component

$$S_n = \frac{f_p d}{(U_o \sin \phi)}$$

(Fig. 3.7b) the value is apparently constant down to angles of 30^o to 40^o.

Any Reynolds number effects on S_n would be disguised by the experimental error, but to allow for its known effect on the Strouhal shedding for right cylinders (cf. Ref. 7 and Fig. 1.2) the final manipulation is to plot in Figure 3.7c.

$$S_n (\phi, Re_n) / S (90^o, Re_n)$$

It was decided that the Reynolds number based on the normal velocity component would be used in this application due to the success of Hanson in collapsing his data with this form. It was found however, that over the range investigated, the particular form of the Reynolds Number used was not very significant since in this range S(Re) is relatively flat (Fig. 1.2). This nondimensionalised normal Strouhal number lies within 10% of unity over the range of reliable data, and it can be seen that this process does collapse the values of S_n found for the right cylinder within 2.5%. The overall deviation from unity is greater than the expected maximum error. In particular, the normalising has produced a disparity between the majority of the data and those at the lowest Re_n. It is not known whether this is a real effect or due to systematic errors introduced in measuring these low velocities. However, the scatter is not sufficient to seriously doubt that the functional relationship

$$S (\phi , Re_n) = S (90^o, Re_n) \sin \phi$$

is a good approximation for the Reynolds numbers examined and for $\phi > 40^o$ (below which the vortex shedding appears to be insignificant).

3.2.3 Peakiness Factor:

Figure 3.8 shows the variation of the peakiness factor with the inclination angle. This factor, which is independent of the stream velocities, simply quantifies the observation from Figure 3.6 that the peaks become ill-defined at small angles. Below 40^o the peak has disappeared into the main spectrum ($R = R_{flat}$, cf. Section 2.4) and the vortex shedding

frequency is no longer a predominant factor in the wake. It is clear that at the limit, with the body axis parallel to the stream direction, no vortex shedding is expected (as from an infinite streamwise wall), thus as the angle approaches this, the dominance must disappear.

It is also of interest to examine whether the shedding actually occurs at a discrete frequency, or whether it is instead dispersed over a narrow bandwidth. Since, from the observed spectral shapes, the 90^{o} case is most likely to exhibit discrete shedding, this case is examined first. From Figure 3.6 the ratio of the peak height to the height of the 'base' spectrum is about 16. Thus $R_{comb} = 0.91$ (Section 2.4). This is the R-value expected if the energy of the shedding were at a single discrete frequency. Since even for the 90^{o} case the experimental value of $R = 0.65$, it must be assumed that at this downstream position the shedding frequency is not discrete, i.e. the thickness of the spectral peak in Figure 3.6 is not entirely a spurious value from the finite filter width. Furthermore, from Fig. 3.11 there is no indication even at 1.1d downstream that the peakiness factor tends to the value 0.91 at the cylinder surface. In the cases for $\phi < 90^{o}$, the broadening of the spectral peaks implies even wider dispersion of the shedding frequency.

3.2.4 Variation of the Spectra with Wake Position for a Right Cylinder:

The decreasing area of the spectral density function in Figure 3.9 indicates that the relative turbulent energy decreases with distance downstream, in agreement with the findings of Section 3.1.3. There is a slight decrease in the peak frequency from 240 cps at 1.1d to 230 cps at 11d, however, Roshko (Ref. 2) did not observe this change and 4% is not very significant. The peak energy is only slightly less than two decades above the 'base' spectrum at 1.1d downstream, while at 11d the peak only rises a third of a decade. This is reflected in the peakiness factor which decreases downstream (Fig. 3.11).

As the probe moves off the centre line, the relative turbulent energy decreases (Figure 3.10), the peak frequency does not change significantly, and the peakiness factor increases slightly. The latter increases 10% from the centre line to the location at which the majority of the measurements were taken, justifying the original choice. The spectrum at the wake centre line indicates an increase in the spectral energy at 400 to 500 cps in comparison with the off-centre spectra. It is possible that the analysis with the Broad filter has again (cf Section 3.2.1) disguised the presence of the second harmonic which would be expected to appear at the centre line due to the effect of the alternate shedding from both sides of the cylinder. In fact the existence of any of the first harmonic in this spectrum suggests the probe was not precisely on the centre line.

3.3 Nondimensionalised Wake Spectra:

By dimensional analysis, the flow field at any point behind a particular body can be described in terms of the nondimensional relationship

$$\frac{\underline{\overline{\phi}}\, f}{U_o^2} = g\left(\frac{fd}{U_o}\right)$$

where $g(fd/U_o)$ is an unknown function and independence of Reynold's Number has been assumed. In this case, the known geometry of the body was used to modify these nondimensional terms. In Section 3.2.2 it was found that $fd/S(90^o, Re_n)\, U_o \sin \phi$ was a preferable nondimensional form for the frequency. Also the spectral density was considered a function of the local mean speed $\overline{U}_w$ in accordance with common turbulence study practice, rather than of the far-removed free stream velocity U_o; although the difference in this case is not large (Section 3.1.1). Further it has been shown (Section 3.1.2) that the energy of the turbulence decreased as $\sin^3 \phi$, and this is to be anticipated to appear in $\underline{\overline{\phi}}$, since $\int_o^\infty \underline{\overline{\phi}}\, df$ is the turbulent energy. The resulting nondimensional form for $\underline{\overline{\phi}}$ is

$$\frac{\underline{\overline{\phi}}\, f}{\overline{U}_w^2 \sin^3 \phi} = h\left(\frac{fd}{S(90^o, Re_n)\, U_o \sin \phi}\right)$$

In Figure 3.12a the results shown in Figure 3.6 are recast in this non-dimensional form, for one speed. Also in Figure 3.12b the results from the low angle tests are presented. The two sets are kept separate since the experimental conditions were not identical. The results are similar but the spectra of the second tests are about a factor of two higher and less well defined for the same angles. However the low angle results are useful to observe the effect of the inclination angle on the spectra.

Figure 3.13 demonstrates the effect of speed on the non-dimensional spectra, for two inclination angles. All the curves for one angle collapse to the same curve near the Strouhal frequency, the peaks being the same height (within the 10% accuracy of the spectral analysis). There appears to be some dependence on speed above and below the peak frequency. For the 90° case, the non-dimensional spectrum decreases by 15% above the peak frequency for the highest speed, while below the peak frequency it increases 30%. This variation is greater than the experimental error and is probably a Reynold's number effect on the drag, hence wake energy, as described in Section 3.1.1. The two speed cases for 52° do not show significant differences.

This non-dimensional form is seen to have approximately collapsed the data for the independent variables, ϕ and U_o, to a common curve <u>below</u> the Strouhal peak, but is unsatisfactory above the peak. It is interesting to compare this with the results of Figure 3.6, which suggest that a good collapse <u>above</u> the Strouhal peak (but not below) can be obtained with the basic non-dimensional relation

$$\frac{\underline{\overline{\phi}}\, f}{\overline{U}_w^2} = g\left(\frac{fd}{U_o}\right)$$

The manipulation of the variables plotted into this latter form merely removes the effect of velocity and does not otherwise affect the 'collapse'.

The collapse for the lower frequencies is understandable due to the strong dependence of the energy at these lower frequencies on the turbulence source, which is the drag. The independence of the collapse from the drag for the higher frequencies suggests that the turbulence at these frequencies is primarily dependent on the viscous mixing of the shear layer, and has not yet been affected by the degeneration of the low frequency eddies.

IV CONCLUSIONS

The Strouhal vortex shedding frequency was found to depend to a good approximation only on the component of velocity normal to a set of inclined circular cylinders, i.e.

$$S = S(90^{o}) \sin \phi$$

and it is believed that this relationship should apply equally well to inclined cylinders of any cross-section.

Also, the energy in the Strouhal peak disperses and decreases in significance with increasing inclination and is virtually submerged in the general wake turbulence spectrum below 40^{o} at a distance of 7.5 diameters downstream of the cylinder.

Various other properties of the wake flow close behind the cylinder were determined as a by-product of the primary Strouhal shedding investigation. The variation of u-component energy with distance downstream was found to follow the fundamental 1/x 'decay law.' Also the u-component energy at a particular distance downstream was found to vary with the drag coefficient and thus with $\sin^{3}\phi$. Furthermore, useful non-dimensionalised representations of the experimental spectra for all inclination angles were found to be, below the shedding frequency

$$\frac{\overline{\phi}\, f}{\overline{U}_{w}^{2} \sin^{3} \phi} = h \left(\frac{f\, d}{S(90^{o},\ Re_{n})\ U_{o} \sin \phi} \right)$$

and above the shedding frequency,

$$\frac{\overline{\phi}\, f}{\overline{U}_{w}^{2}} = g \left(\frac{f\, d}{U_{o}} \right)$$

REFERENCES

1. Hanson, A. R. — Vortex Shedding from Yawed Cylinders, AIAA J., 4, 4, 738, April 1966.

2. Roshko, A. — On the Development of Turbulent Wakes From Vortex Streets, NACA Rept. 1191, 1954.

3. Surry, J. — Experimental Investigation of the Characteristics of Flow about Curved Circular Cylinders. UTIAS TN 89, April 1965.

4. Relf, E. F. Powell, C. H. — Tests on Smooth and Stranded Wires Inclined to the Wind Direction, and a Comparison of Results on Stranded Wires in Air and Water, ARC, R & M. 307, 1917,

5. Sears, W. R. — Boundary Layer of Yawed Cylinders, J. of Aero. Sci., 15, 1, 491, January 1948.

6. Bursnall, W. J. Loftin, L. K. — Experimental Investigation of the Pressure Distribution About a Yawed Circular in the Critical Reynold's Number Range, NACA 2463, 1951.

7. Etkin, B. Korbacher, G. K. Keefe, R. T. — Acoustic Radiation from a Stationary Cylinder in a Fluid Stream (Aedian Tones), UTIAS Rept. 39, May 1956.

8. Roshko, A. — On the Drag and Shedding Frequency of Two-Dimensional Bluff Bodies, NACA TN 3169, July 1954.

9. Hinze — Turbulence: An Introduction to Its Mechanism and Theory, McGraw Hill, N.Y., 1959.

10. Townsend, A. A. — The Structure of Turbulent Shear Flow, Cambridge Univ. Press, 1956.

APPENDIX

The Expected Value of R When the Experimental Spectrum is a Combination of a Flat Base Spectrum and a Single Discrete Peak

Consider the sketches below. The sketch on the left indicates the assumed input spectrum consisting of a flat base spectrum and a discrete signal at f_p. The energy in the discrete signal is $e^2(f_p)$. The sketch on the right indicates the type of output that would be experimentally obtained if this signal were analysed with wave analysers of Narrow bandwidth G_N and Broad bandwidth G_B.

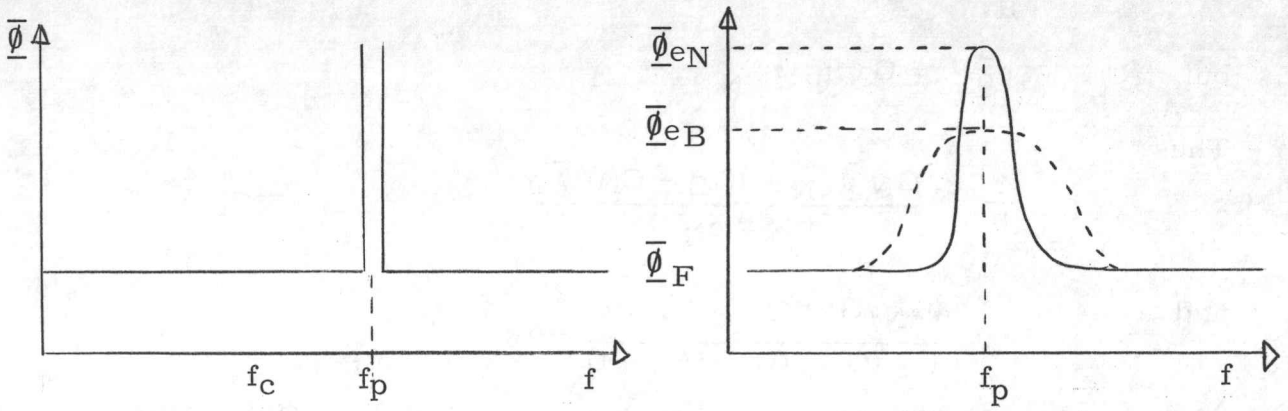

There are then three experimentally determined parameters. They are the peak values obtained through each wave analyser bandwidth ($\overline{\phi}\, e_N$ and $\overline{\phi} e_B$) and the flat value ($\overline{\phi}_F$) obtained far removed from the peak. Thus if the above model of the combined spectrum is assumed, a knowledge of $\overline{\phi} e_N$ and $\overline{\phi}_F$ should enable $\overline{\phi} e_B$ to be predicted and hence also the expected value of R_{comb} (see Section 2.2 for the definition of R). If this value of the peakiness factor does not agree with the experimentally determined value, then we can conclude that it is unlikely that the true spectrum actually contains a discrete peak.

Theoretically, the mean square output obtained through a wave analyser of characteristics g and G, centered at f_c (see List of Symbols for definitions of the terms), will be:

$$e_o^2(f_c; g) = \int_o^\infty f_c\, g\, \overline{\phi}_F \frac{df}{f_c} + g\left(\frac{f_p}{f_c}\right) e^2(f_p)$$

$$= f_c\, G\, \overline{\phi}_F + g\left(\frac{f_p}{f_c}\right) e^2(f_p)$$

and thus

$$e_o^2(f_p; g) = f_p\, G\, \overline{\phi}_F + e^2(f_p)$$

but by definition

$$\underline{\overline{\phi}}_e (f_c ; G) = e_o^2 (f_c ; G) / G f_c$$

and thus

$$\underline{\overline{\phi}}_e (f_p ; G) = \underline{\overline{\phi}}_F + e^2 (f_p) / G f_p$$

Now, if both wave analyser bandwidths are considered:

$$e^2 (f_p) = e_{oN}^2 (f_p ; g_N) - f_p G_N \underline{\overline{\phi}}_F = e_{o\,B}^2 (f_p ; g_B) - f_p G_B \underline{\overline{\phi}}_F$$

Then

$$\frac{1}{R} = e_{oB}^2 / e_{oN}^2 = 1 + f_p \underline{\overline{\phi}}_F (G_B - G_N) / e_{oN}^2$$

but

$$e_{oN}^2 = G_N f_p \underline{\overline{\phi}}_{e_N}$$

Thus

$$\frac{1}{R} = \frac{G_N \underline{\overline{\phi}}_{e_N} + (G_B - G_N) \underline{\overline{\phi}}_F}{G_N \underline{\overline{\phi}}_{e_N}}$$

and

$$R = \frac{(G_N / G_B) \epsilon}{1 + (G_N / G_B)(\epsilon - 1)}$$

where

$$\epsilon = \underline{\overline{\phi}}_{e_N} / \underline{\overline{\phi}}_F$$

This final expression reduces to the two limits mentioned in Section 2.4 of the text of

$$R = G_N / G_B \quad \text{for } \epsilon = 1, \text{ and } R = 1 \quad \text{for } \underline{\overline{\phi}}_F = 0$$

It might be noted that this expression actually holds more generally than just for a flat base spectrum. As long as the function $g(f/f_c)$ for the wave analyser is symmetrical with frequency, then the above will hold provided $\underline{\overline{\phi}}_F$ is antisymmetrical with frequency about $(f_p , \underline{\overline{\phi}}_F (f_p))$. This can usually be a reasonable approximation over the narrow frequency range of the filter.

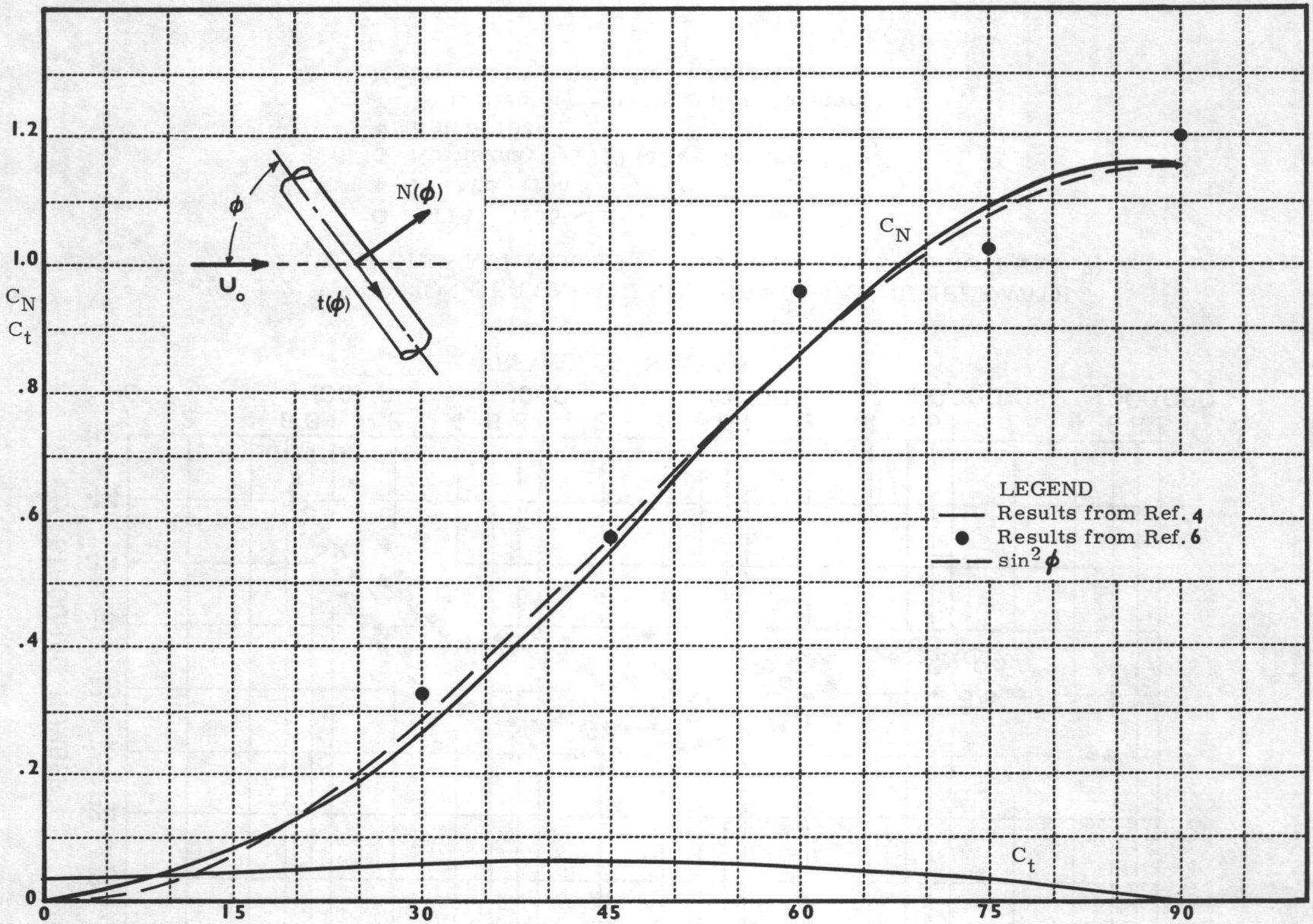

FIG. 1.1 VARIATION OF NORMAL AND TANGENTIAL FORCE COEFFICIENTS OF A CIRCULAR CYLINDER WITH INCLINATION ANGLE

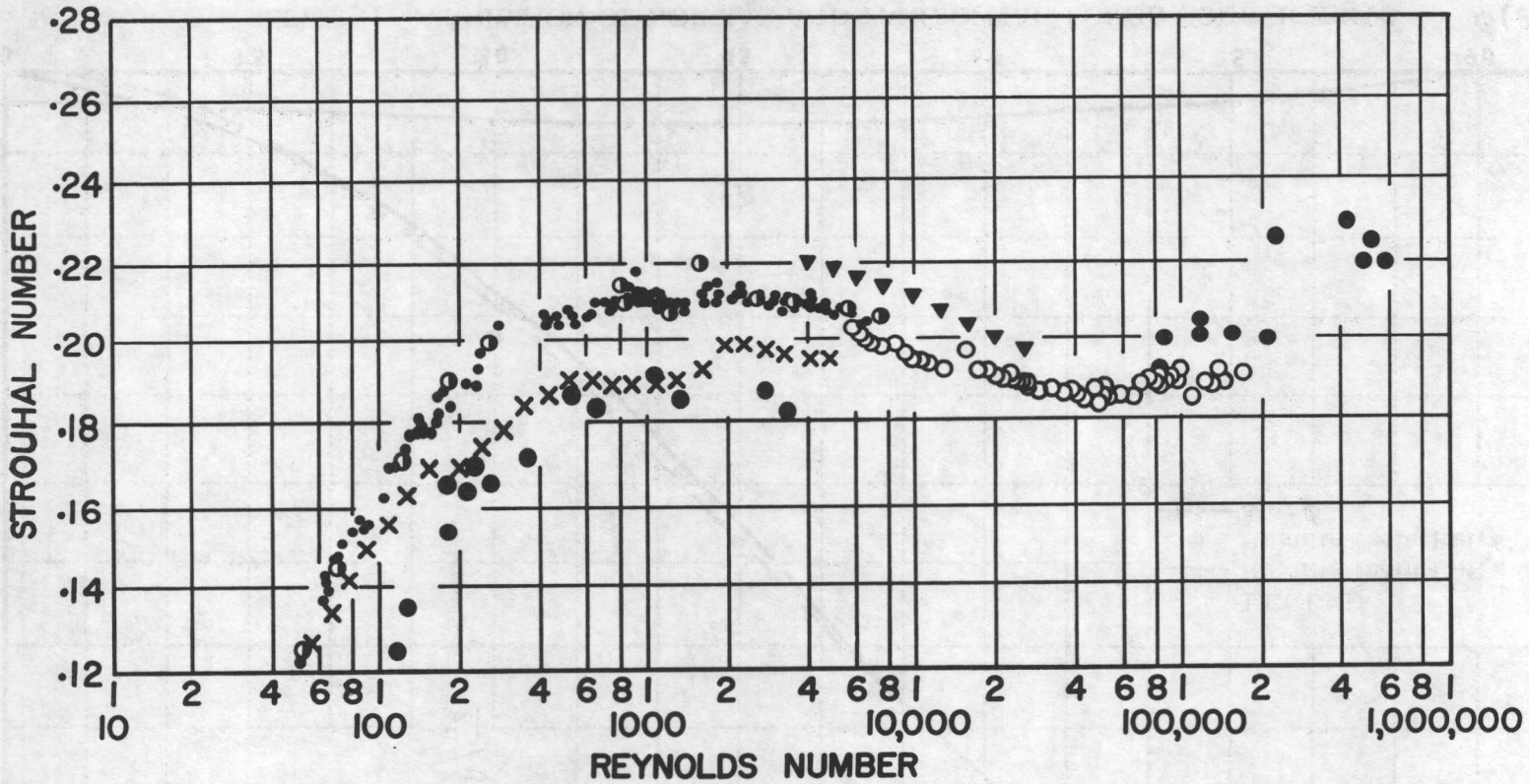

FIG. 1.2 VARIATION OF FUNDAMENTAL STROUHAL NUMBER WITH REYNOLDS NUMBER FOR A RIGHT CYLINDER (FROM REF. 7)

- ○ UTIA - 1955
- • Roshko - 1953
- ◑ Kovasznay - 1949 (after Roshko)
- ● Relf - 1924
- ▼ DVL Hiebtone - 1919 (after Lehnert)
- × Strouhal - 1878 (after Lehnert)

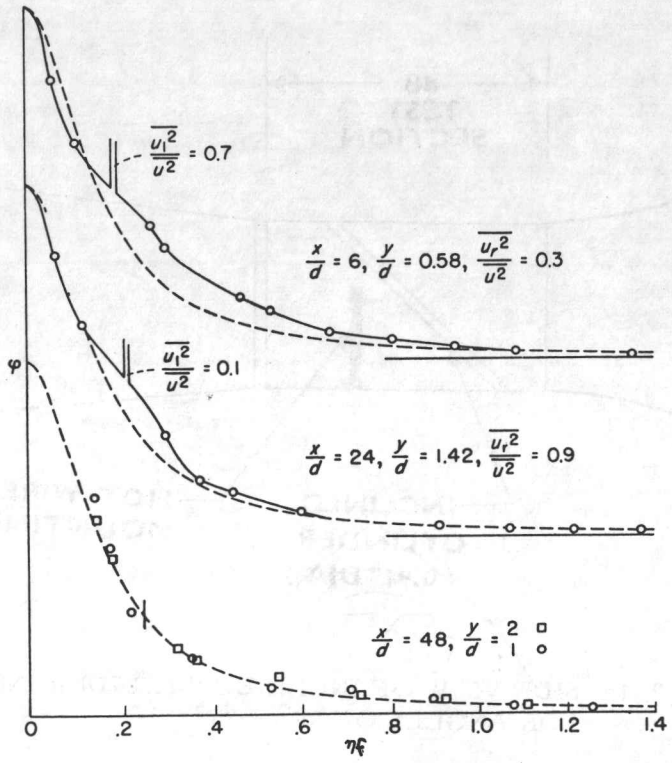

Reference Curve $\Phi = \frac{4}{1 + (2 \pi \eta f)^2}$

η is a nondimensionalizing factor

$\overline{u_1^2} / \overline{u^2}$ = fraction of u-component turbulence energy contained in Strouhal peak

$\frac{\overline{u_r^2}}{u^2} = 1 - \frac{\overline{u_1^2}}{u^2}$

FIG. 1.3 DOWNSTREAM DEVELOPMENT OF THE TURBULENCE SPECTRUM BEHIND A RIGHT CIRCULAR CYLINDER AT A REYNOLDS NUMBER OF 4000 (From Ref. 2)

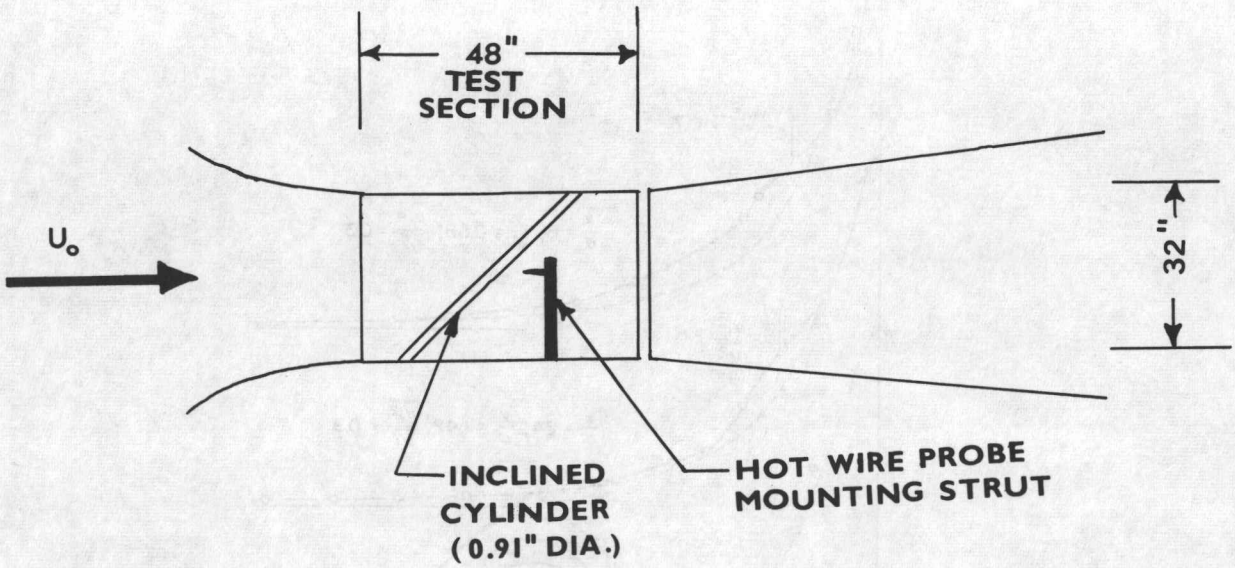

FIG. 2.1a SIDE VIEW OF INCLINED CYLINDER INSTALLATION FOR ANGLES OF 90° - 35°

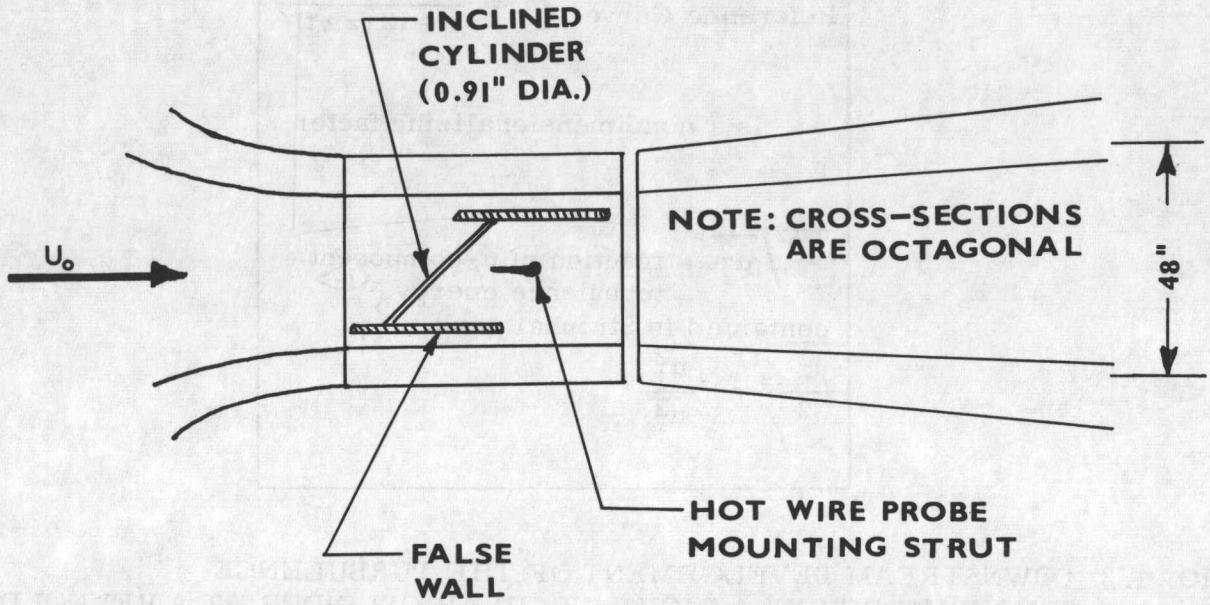

FIG. 2.1b TOP VIEW OF INCLINED CYLINDER INSTALLATION FOR ANGLES OF 42° - 10°

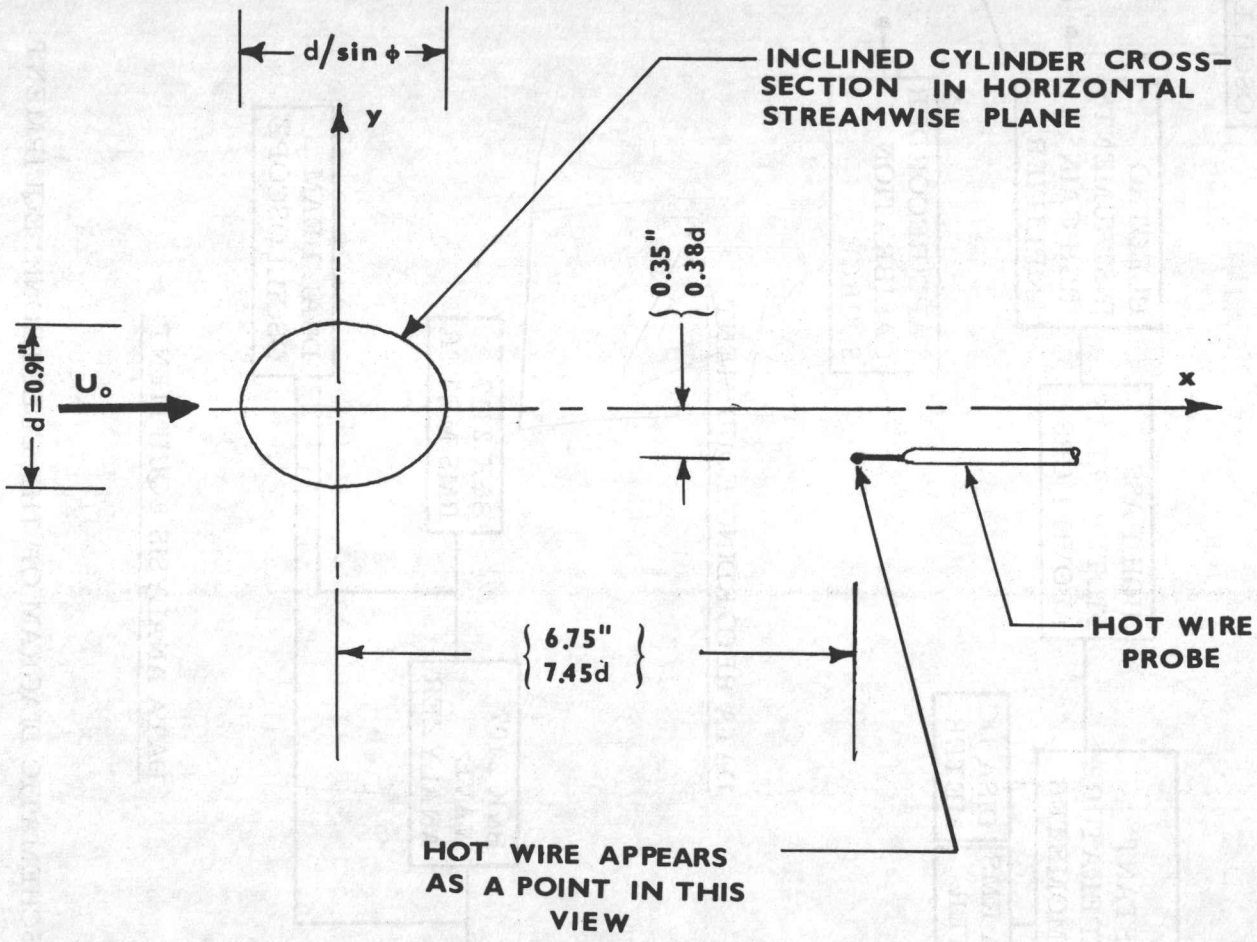

FIG. 2.2 PRINCIPLE LOCATION OF HOT WIRE PROBE IN THE WAKE

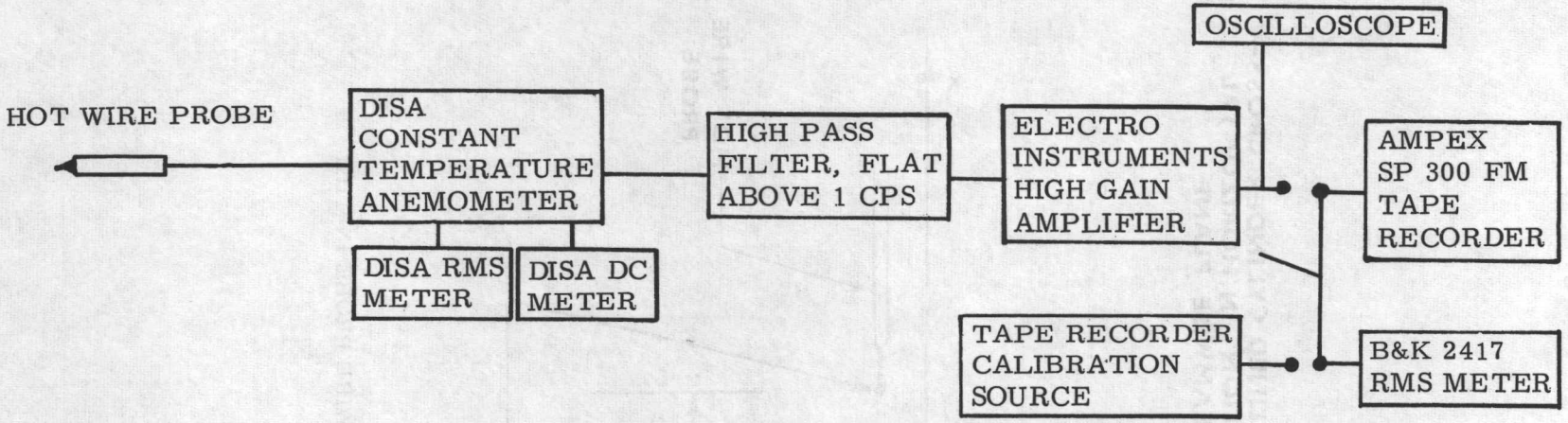

DATA RECORDING EQUIPMENT

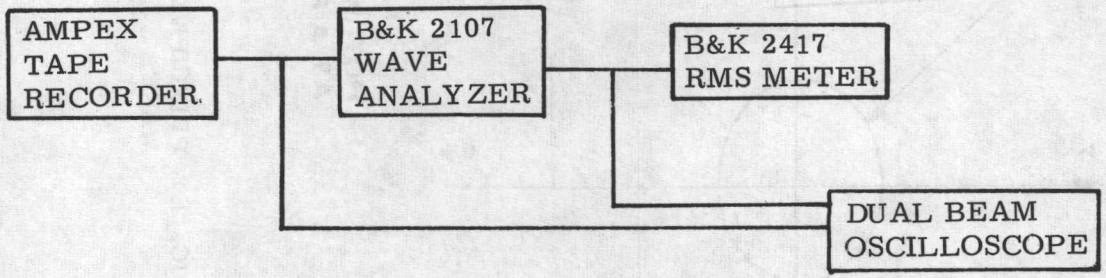

DATA ANALYSIS EQUIPMENT

FIG. 2.3 SCHEMATIC DIAGRAM OF THE ELECTRONIC EQUIPMENT

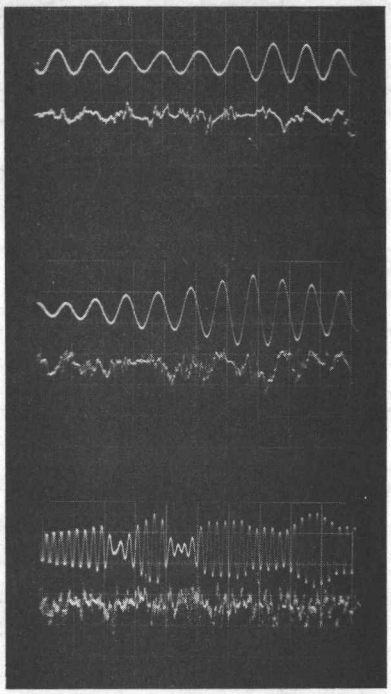

FIG. 3.1 TYPICAL HOT WIRE SIGNALS OF WAKE TURBULENCE BEHIND A RIGHT CIRCULAR CYLINDER AT x/d=11, y/d=1.1

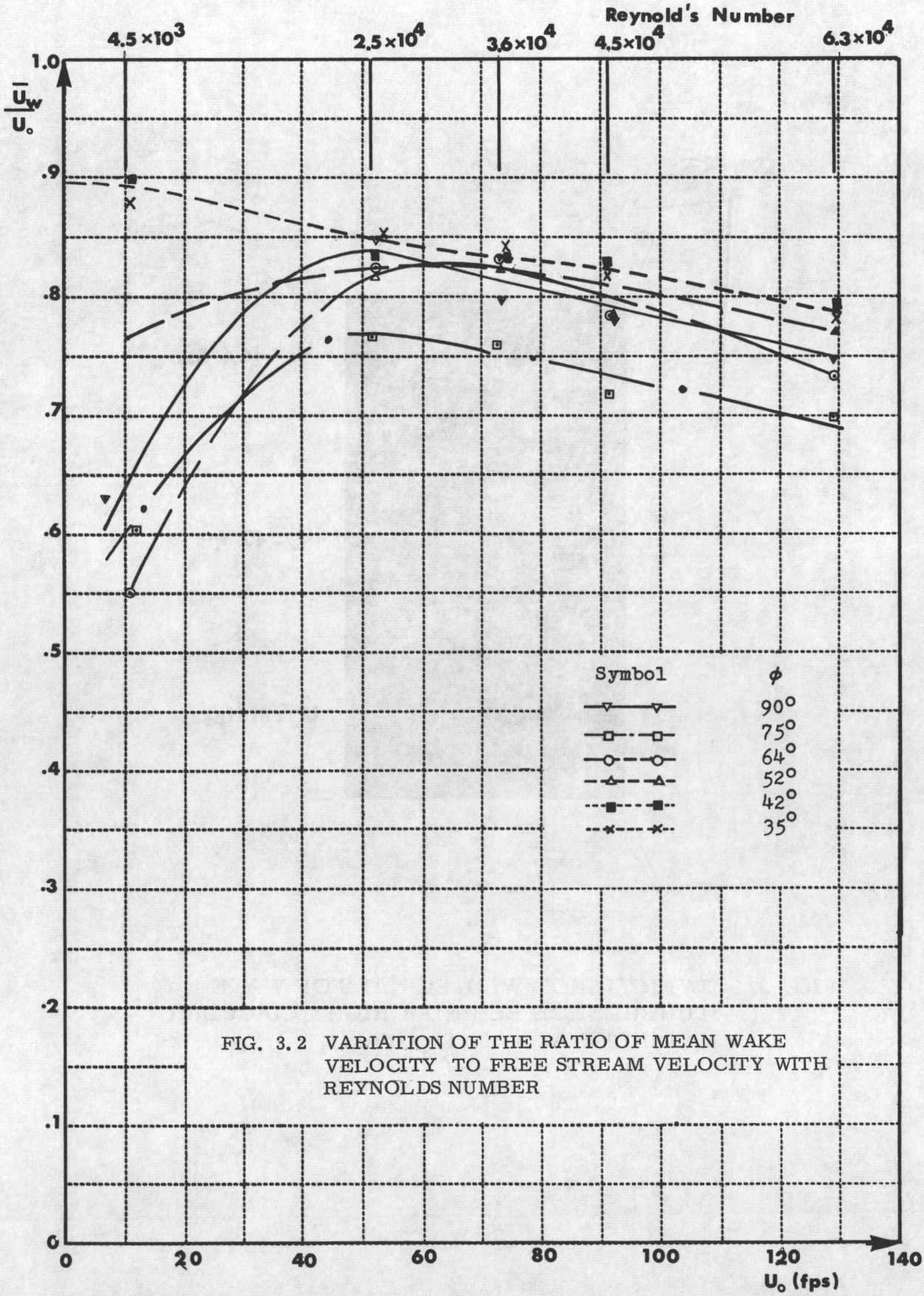

FIG. 3.2 VARIATION OF THE RATIO OF MEAN WAKE VELOCITY TO FREE STREAM VELOCITY WITH REYNOLDS NUMBER

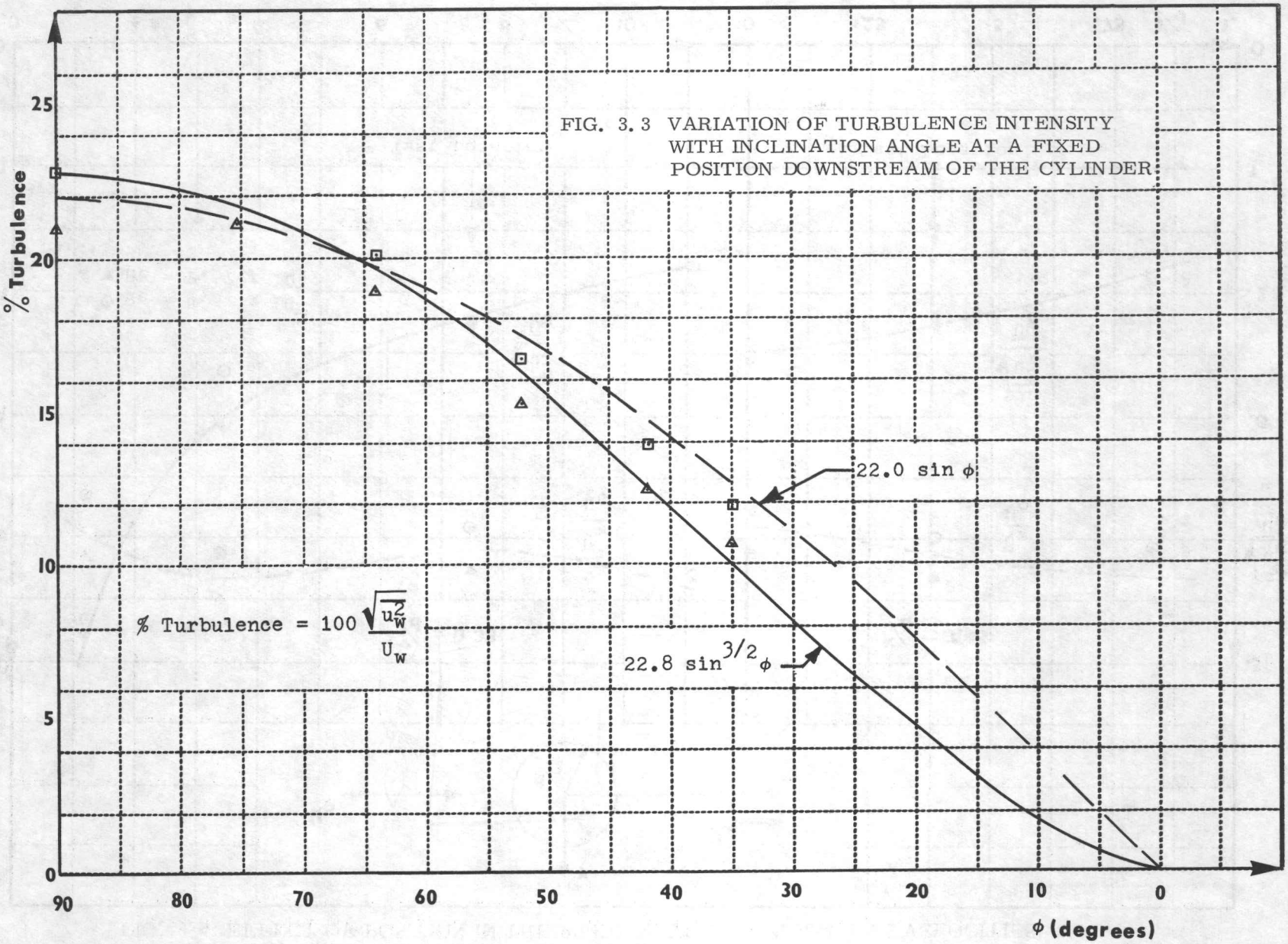

FIG. 3.3 VARIATION OF TURBULENCE INTENSITY WITH INCLINATION ANGLE AT A FIXED POSITION DOWNSTREAM OF THE CYLINDER

FIG. 3.4 EFFECT OF POSITION IN THE WAKE ON THE MEAN AND RMS VELOCITIES

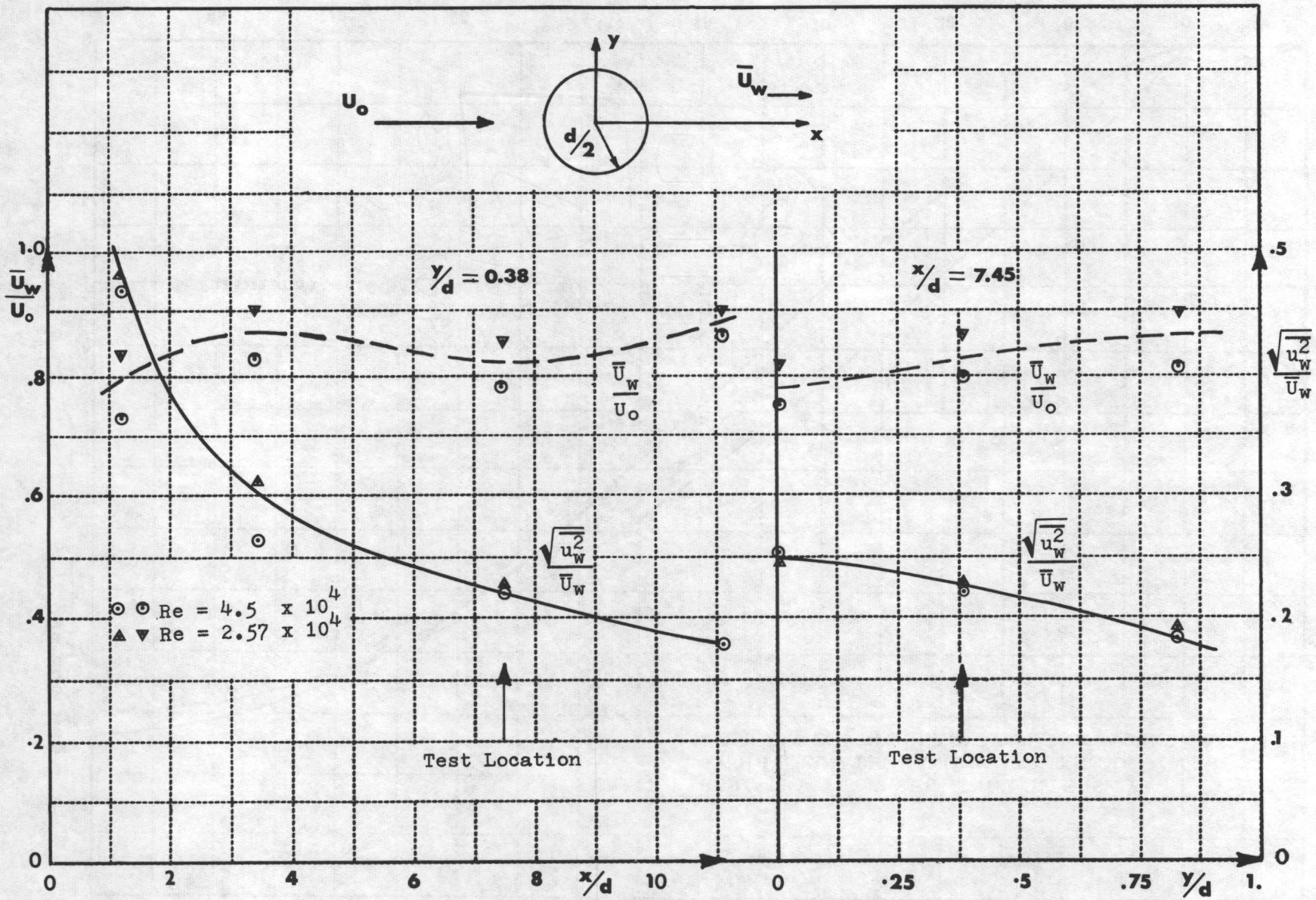

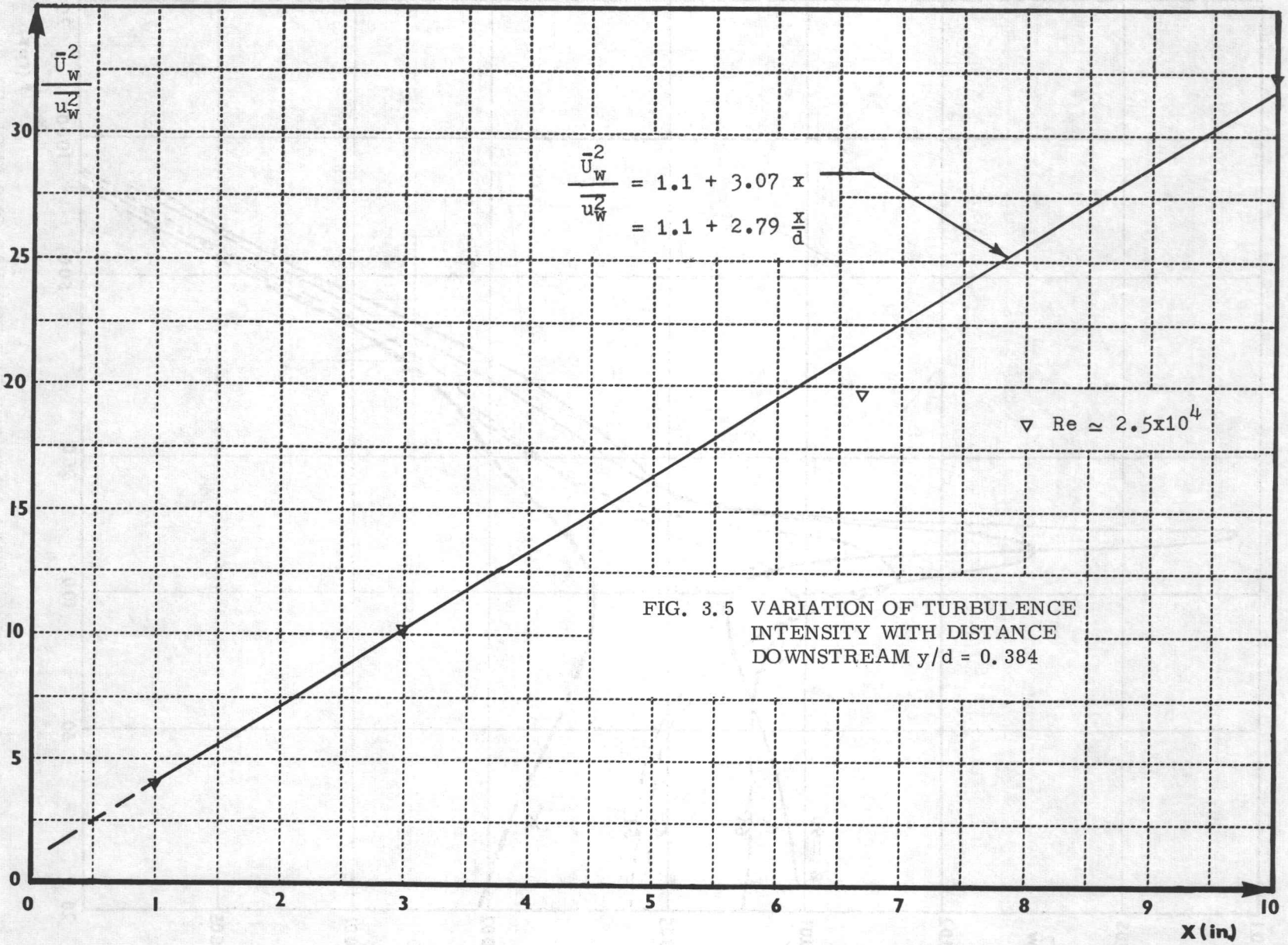

FIG. 3.5 VARIATION OF TURBULENCE INTENSITY WITH DISTANCE DOWNSTREAM y/d = 0.384

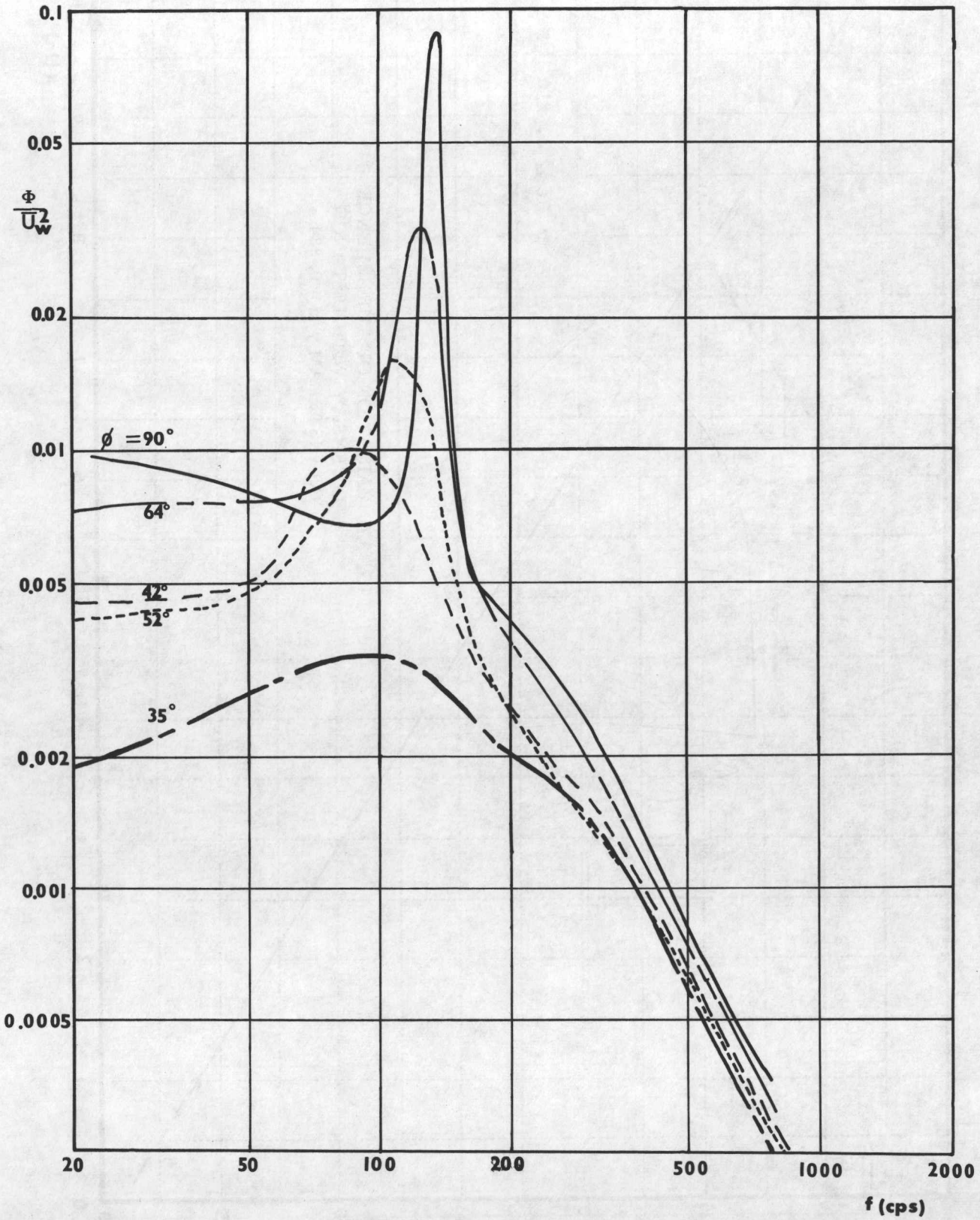

FIG. 3.6 WAKE SPECTRA AT ONE SPEED FOR VARIOUS ANGLES OF INCLINATION ($x/d=7.45$, $y/d=0.38$, $Re=2.57 \times 10^4$)

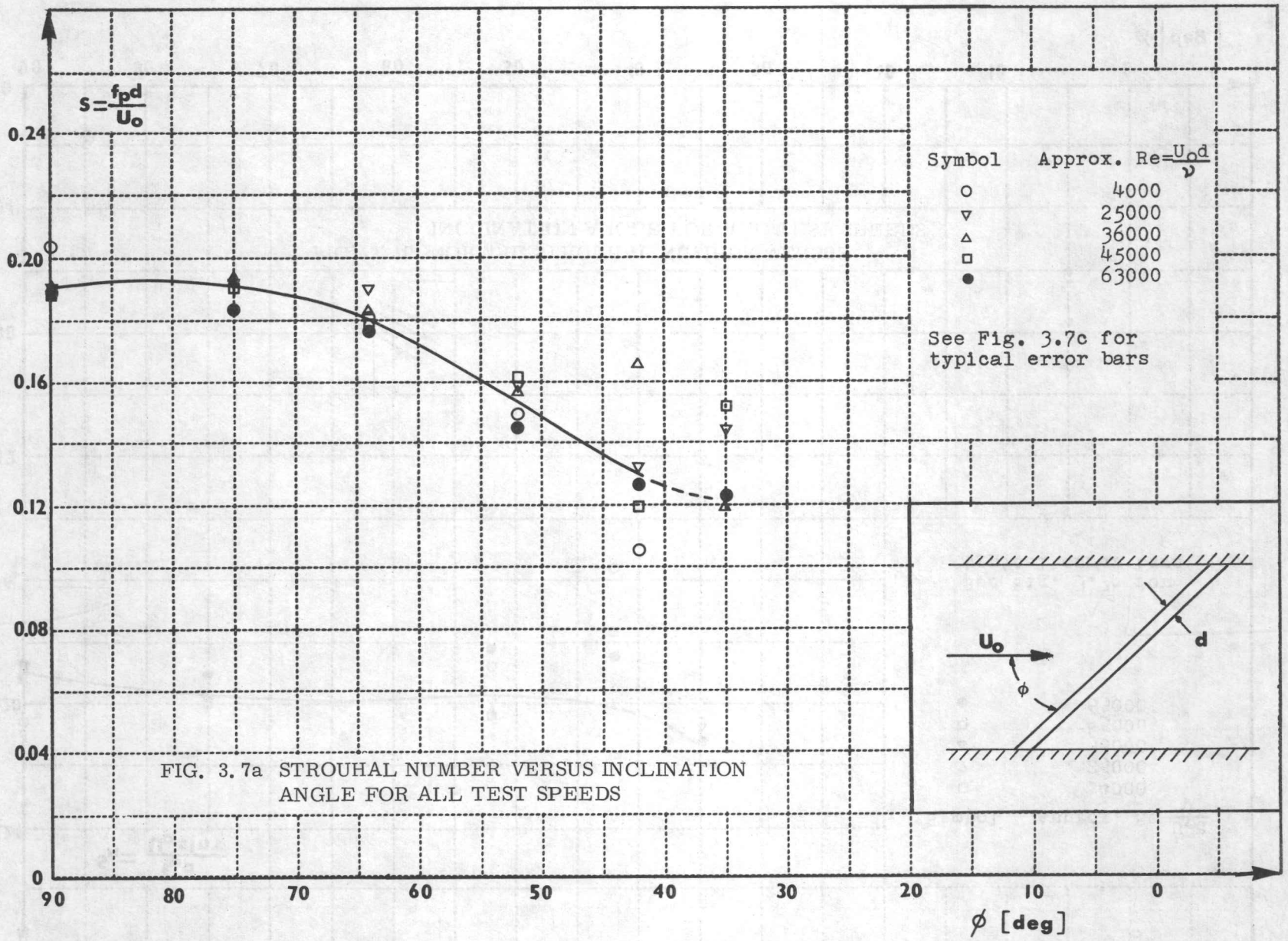

FIG. 3.7a STROUHAL NUMBER VERSUS INCLINATION ANGLE FOR ALL TEST SPEEDS

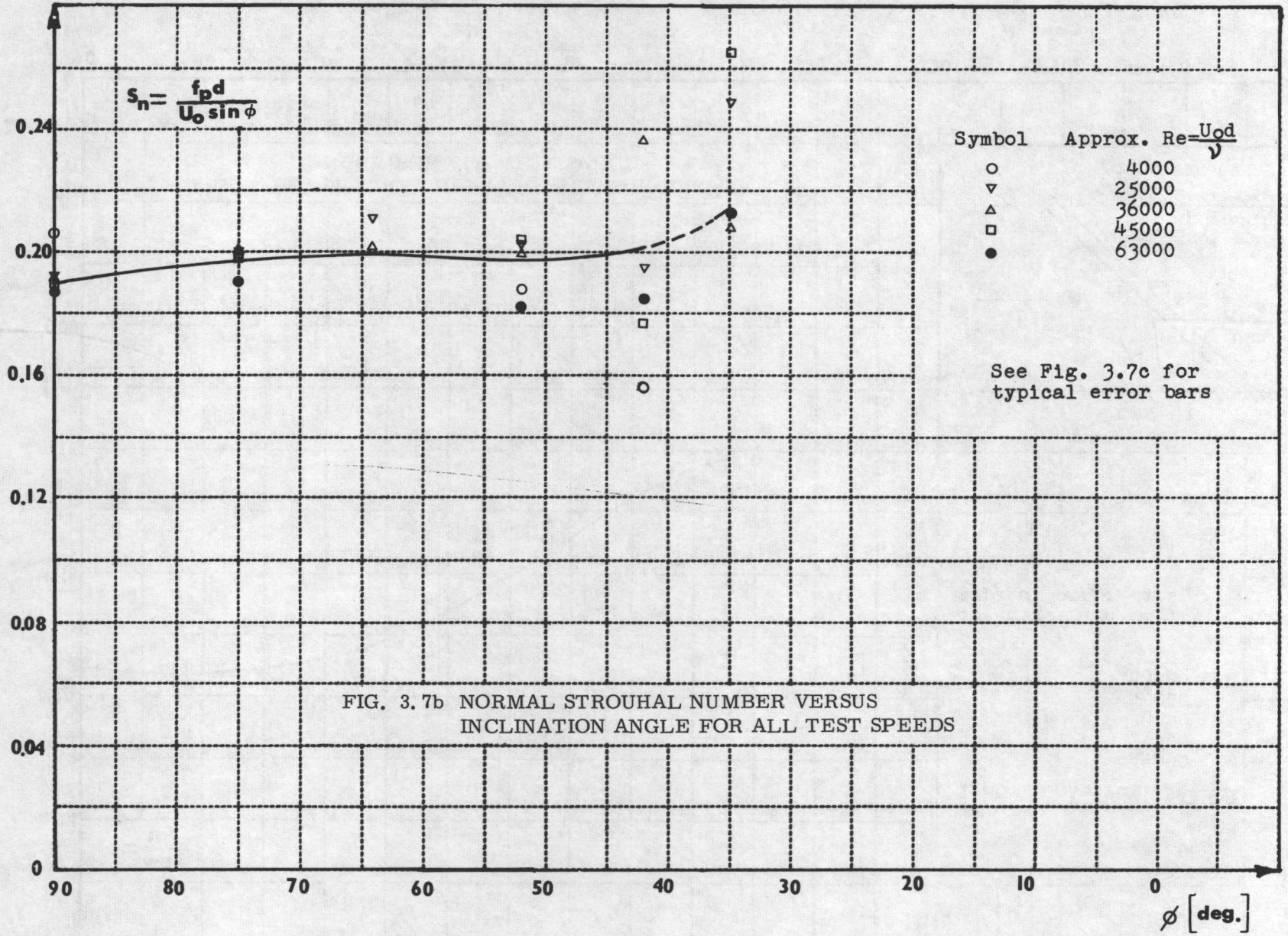

FIG. 3.7b NORMAL STROUHAL NUMBER VERSUS INCLINATION ANGLE FOR ALL TEST SPEEDS

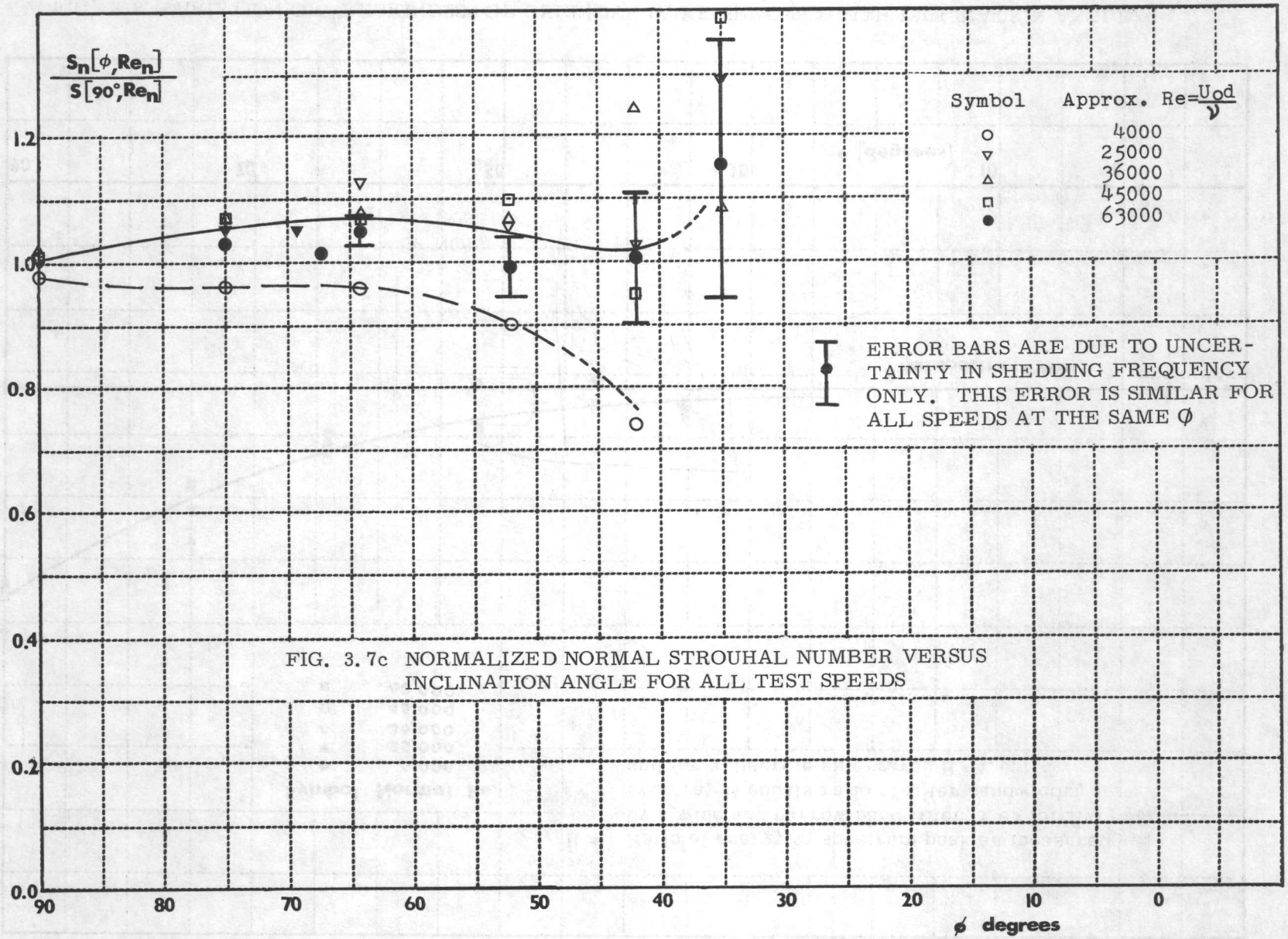

FIG. 3.7c NORMALIZED NORMAL STROUHAL NUMBER VERSUS INCLINATION ANGLE FOR ALL TEST SPEEDS

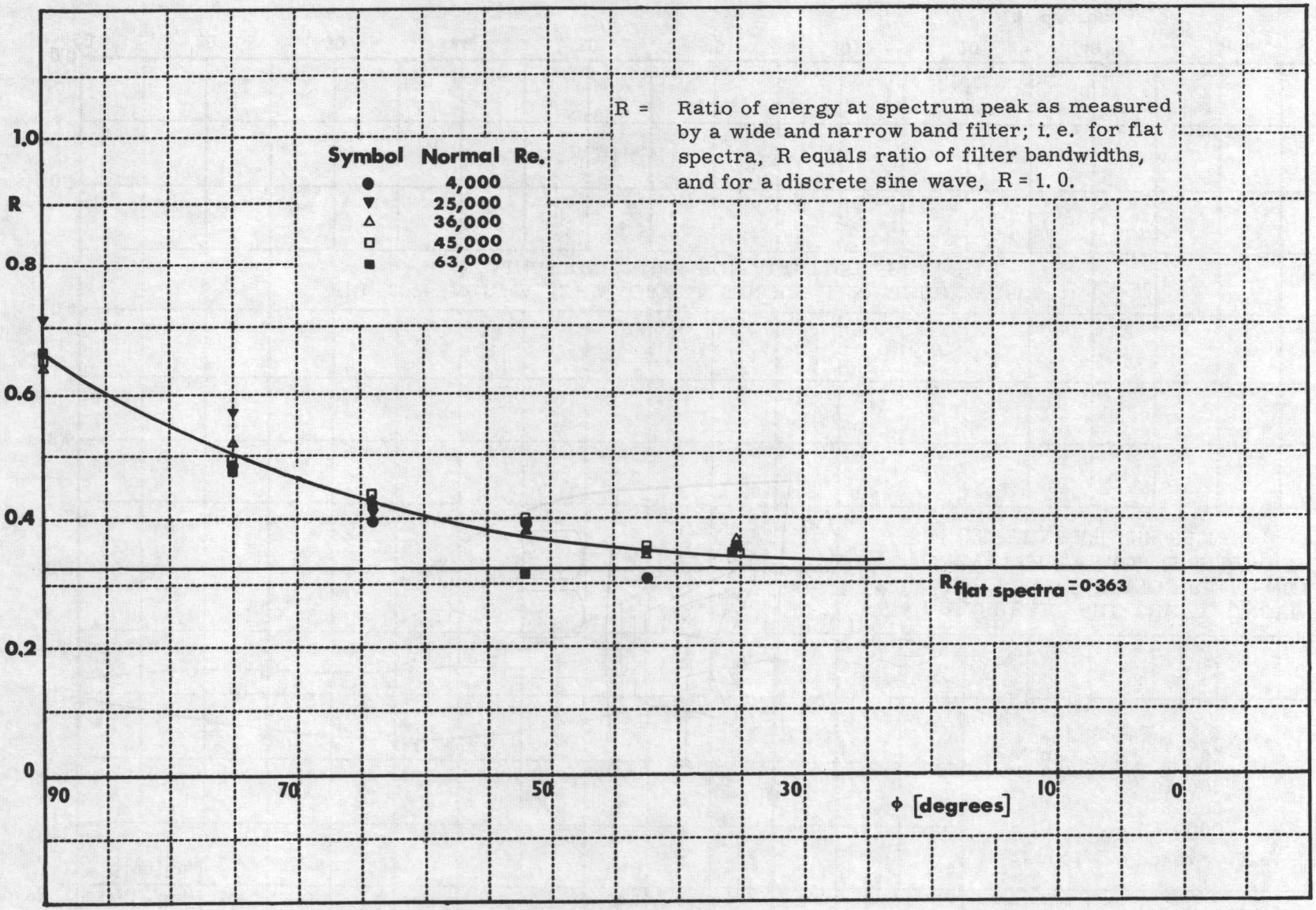

FIG. 3.8 VARIATION OF "PEAKINESS" OF CYLINDER WAKE SPECTRA WITH INCLINATION ANGLE

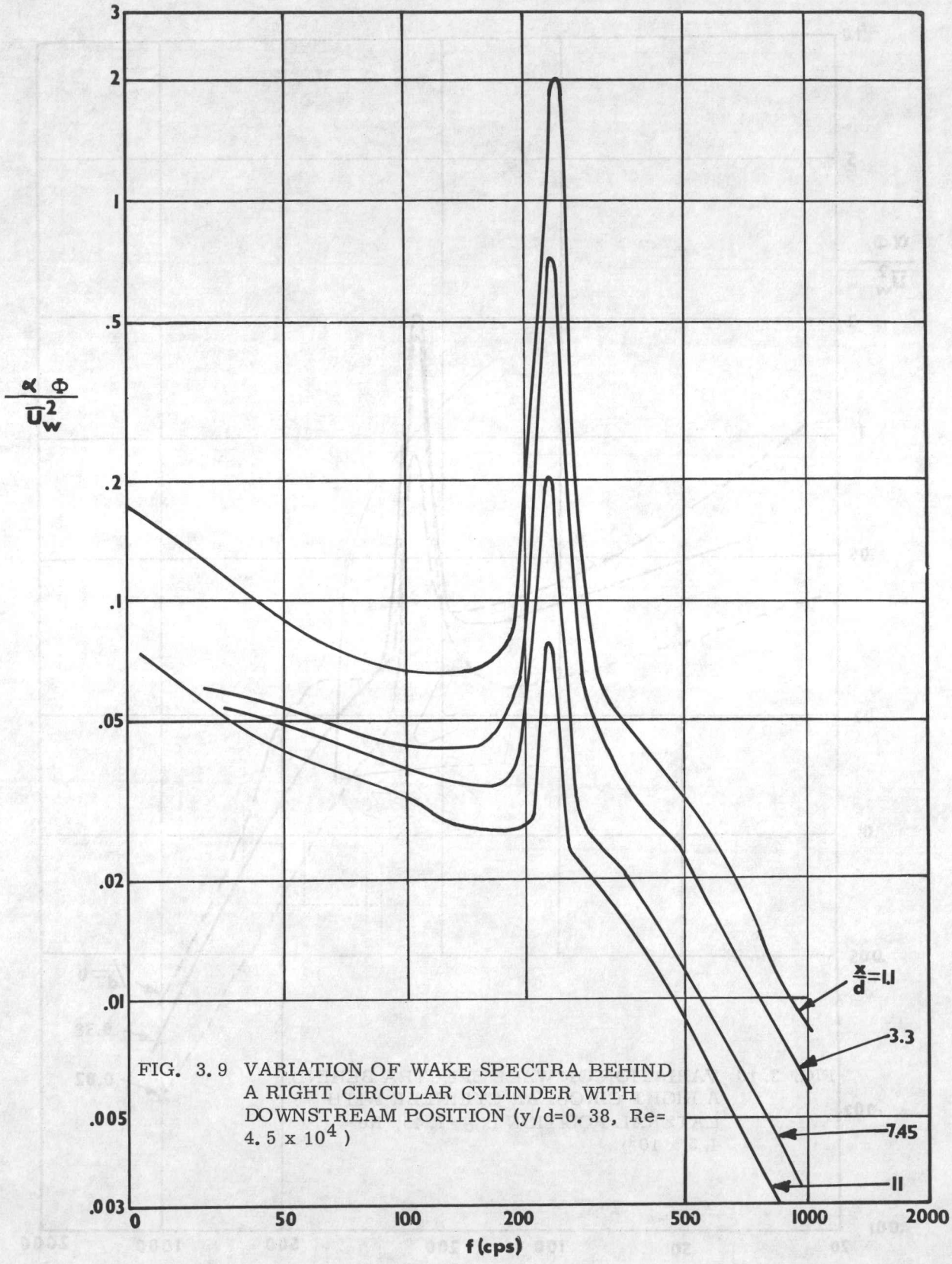

FIG. 3.9 VARIATION OF WAKE SPECTRA BEHIND A RIGHT CIRCULAR CYLINDER WITH DOWNSTREAM POSITION (y/d=0.38, Re= 4.5×10^4)

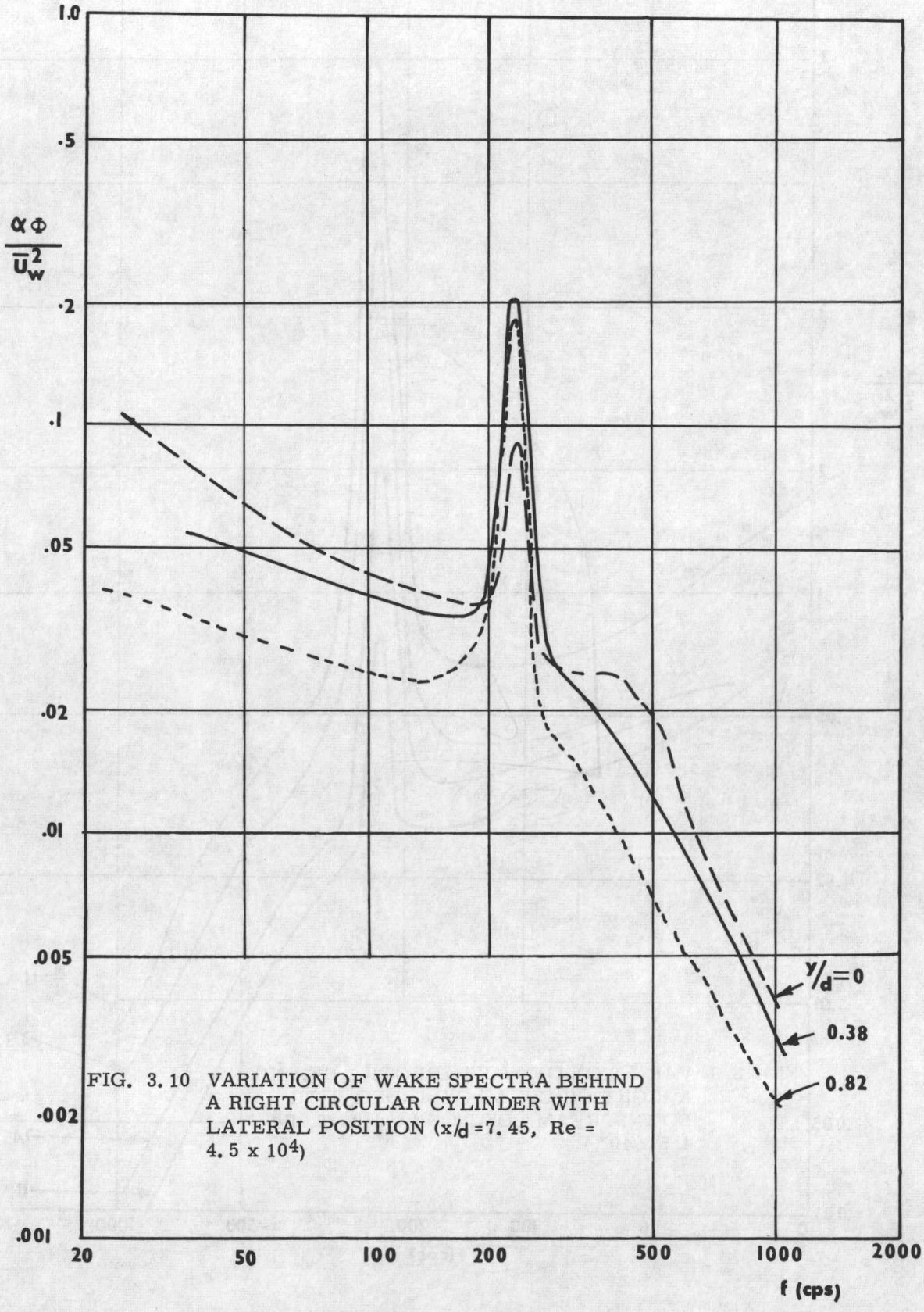

FIG. 3.10 VARIATION OF WAKE SPECTRA BEHIND A RIGHT CIRCULAR CYLINDER WITH LATERAL POSITION ($x/d = 7.45$, $Re = 4.5 \times 10^4$)

FIG. 3.11 VARIATION OF "PEAKINESS" OF THE RIGHT CYLINDER WAKE SPECTRA WITH POSITION IN THE WAKE (Re = 4.5×10^4)

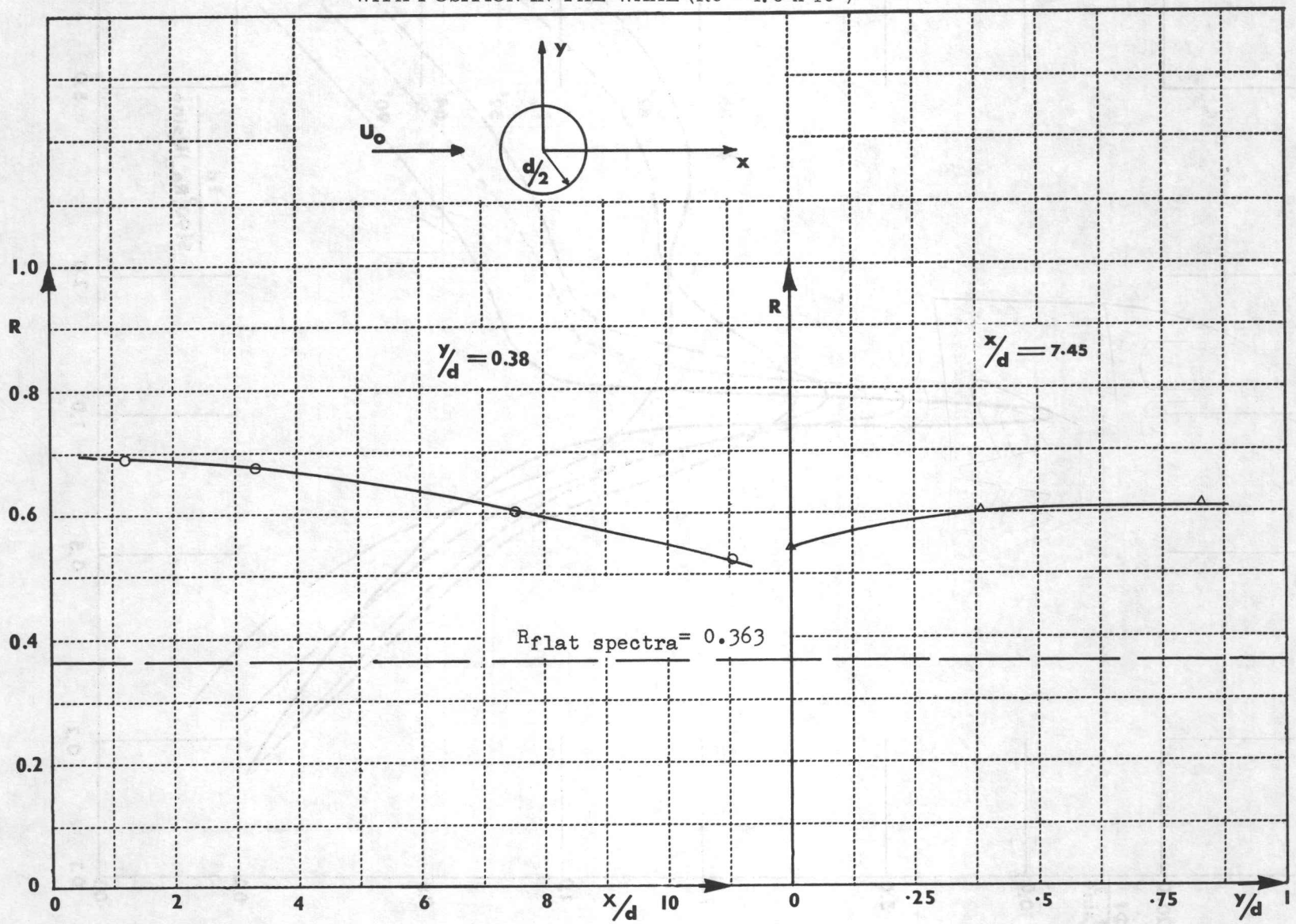

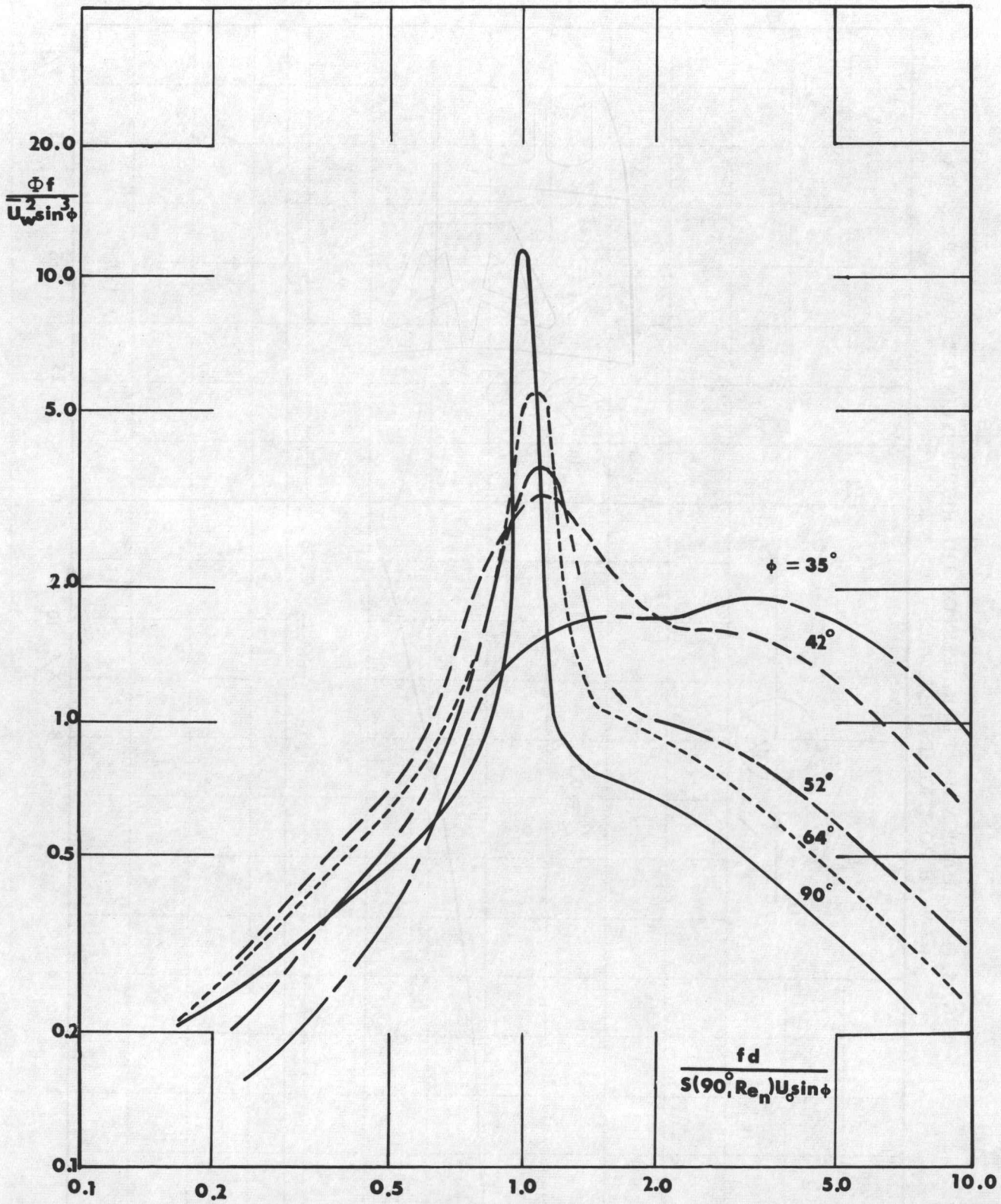

FIG. 3.12a NONDIMENSIONAL WAKE SPECTRA AT ONE SPEED FOR INCLINATION ANGLES FROM 90° to 35°. (x/d=7.45, y/d=0.38, Re=2.57 x 10^4)

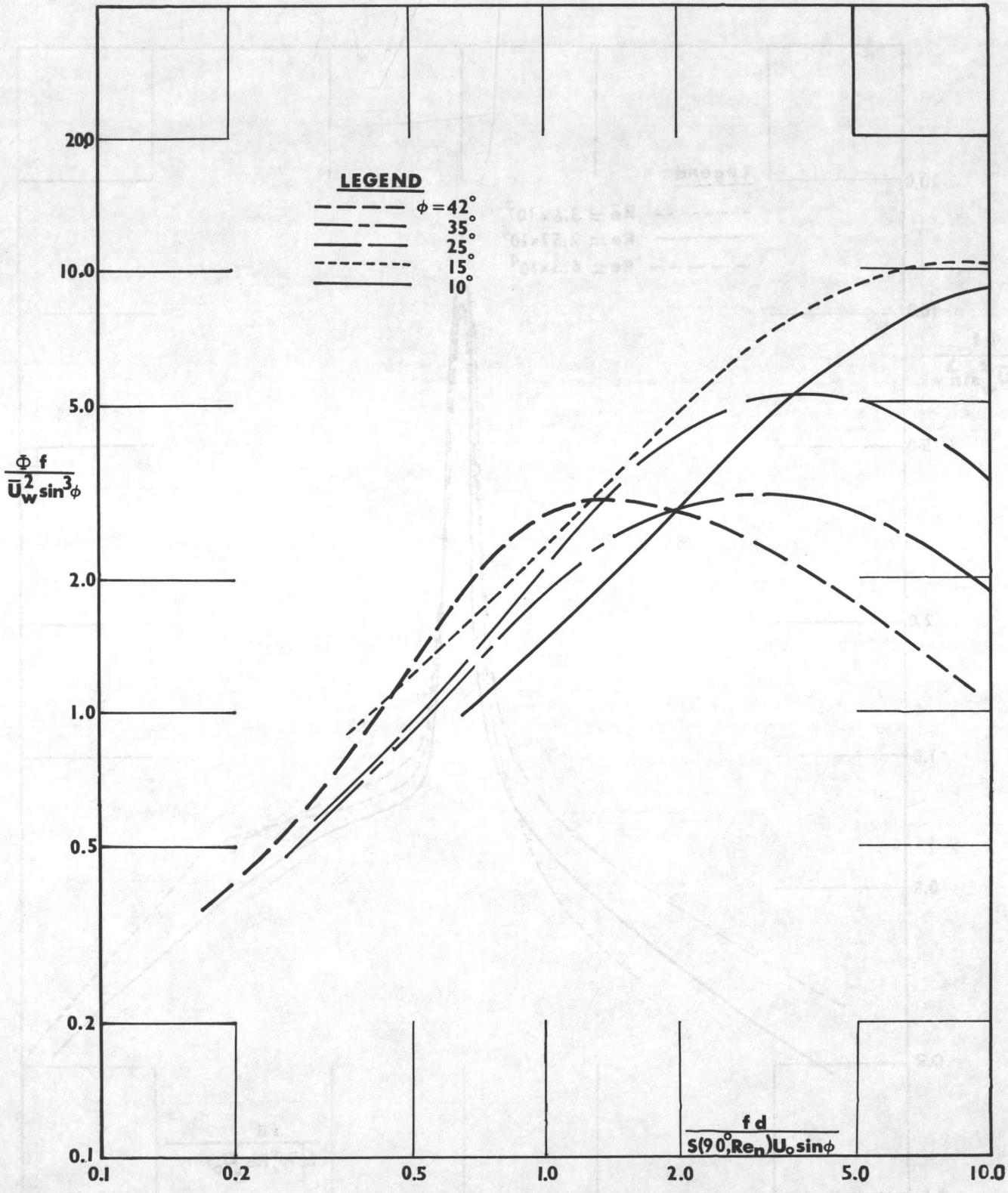

FIG. 3.12b NONDIMENSIONAL WAKE SPECTRA AT ONE SPEED FOR INCLINATION ANGLES FROM 42^o to 10^o ($x/d=7.45$, $y/d=0.47$, $Re=2.57 \times 10^4$)

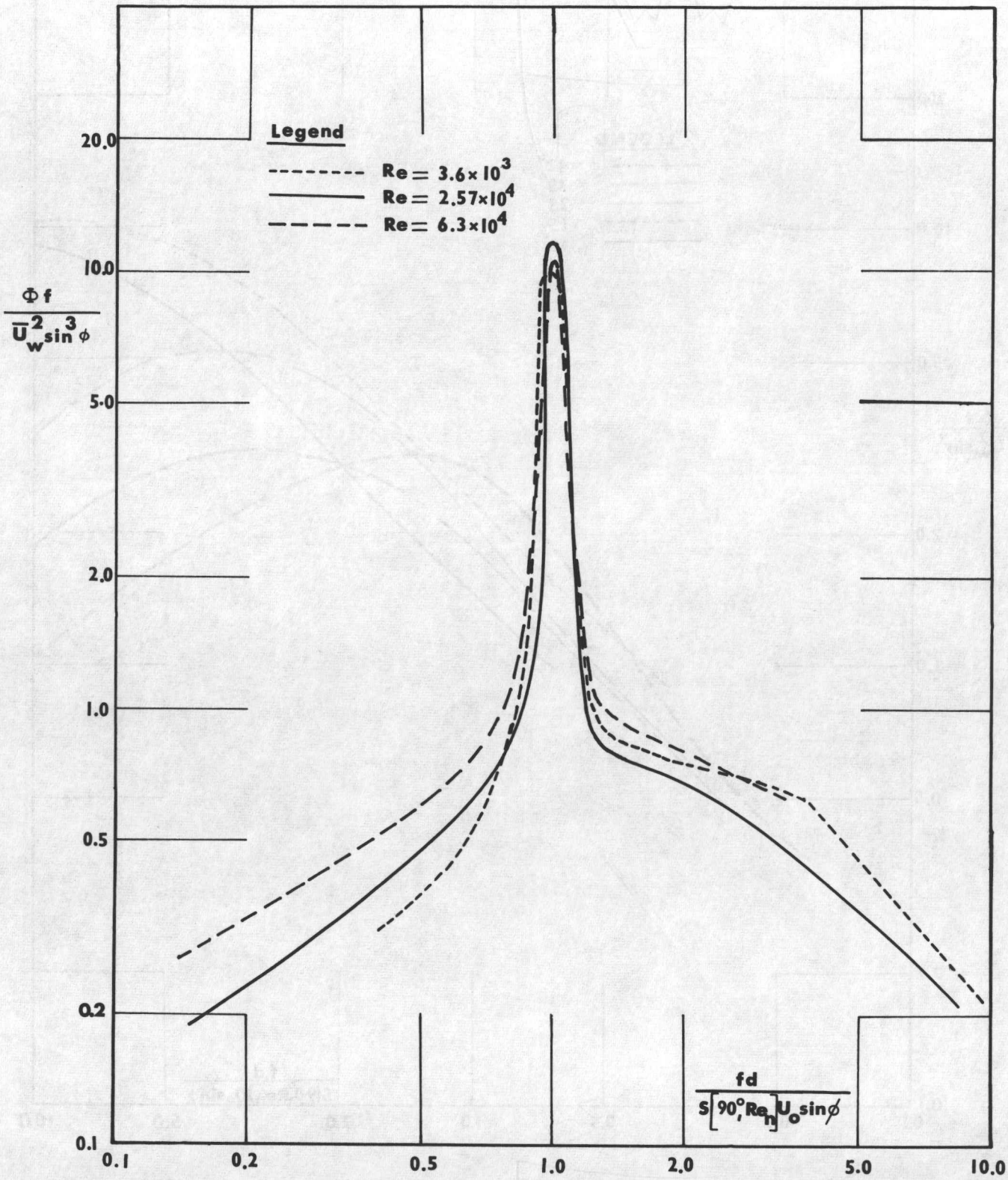

FIG. 3.13a NONDIMENSIONAL WAKE SPECTRA BEHIND THE 90° CYLINDER AT VARIOUS SPEEDS (x/d = 7.45, y/d = 0.38)

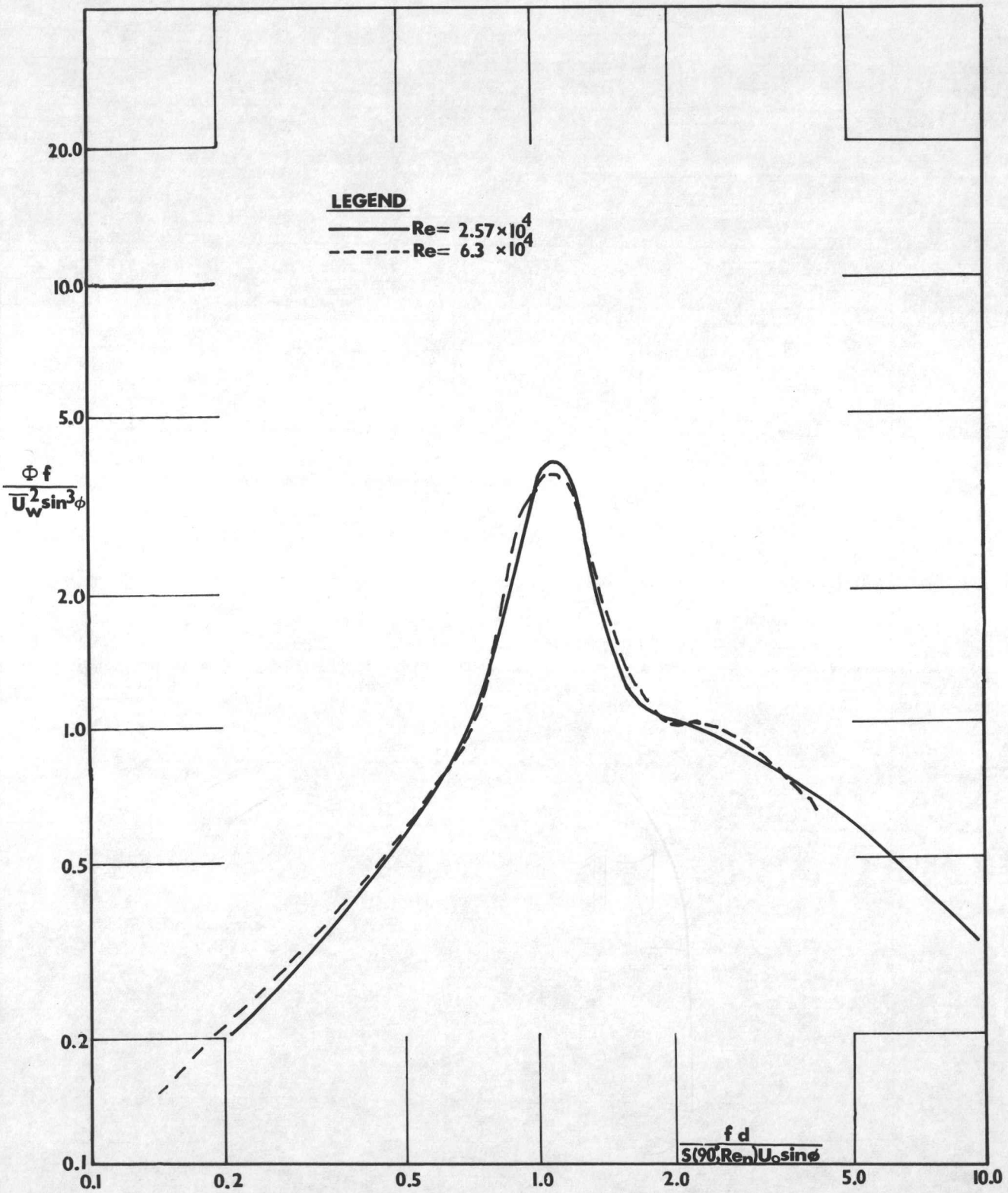

FIG. 3.13b NONDIMENSIONAL WAKE SPECTRA BEHIND THE 52° CYLINDER AT TWO SPEEDS (x/d = 7.45, y/d = 0.38)